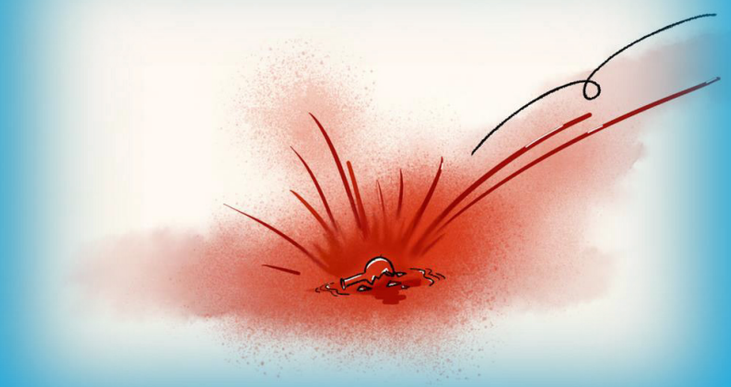

Triplet state access in multi-component heavy atom free photosensitizers in photomedicine

Dáire J. Gibbons

Triplet state access in multi-component heavy atom free photosensitizers in photomedicine

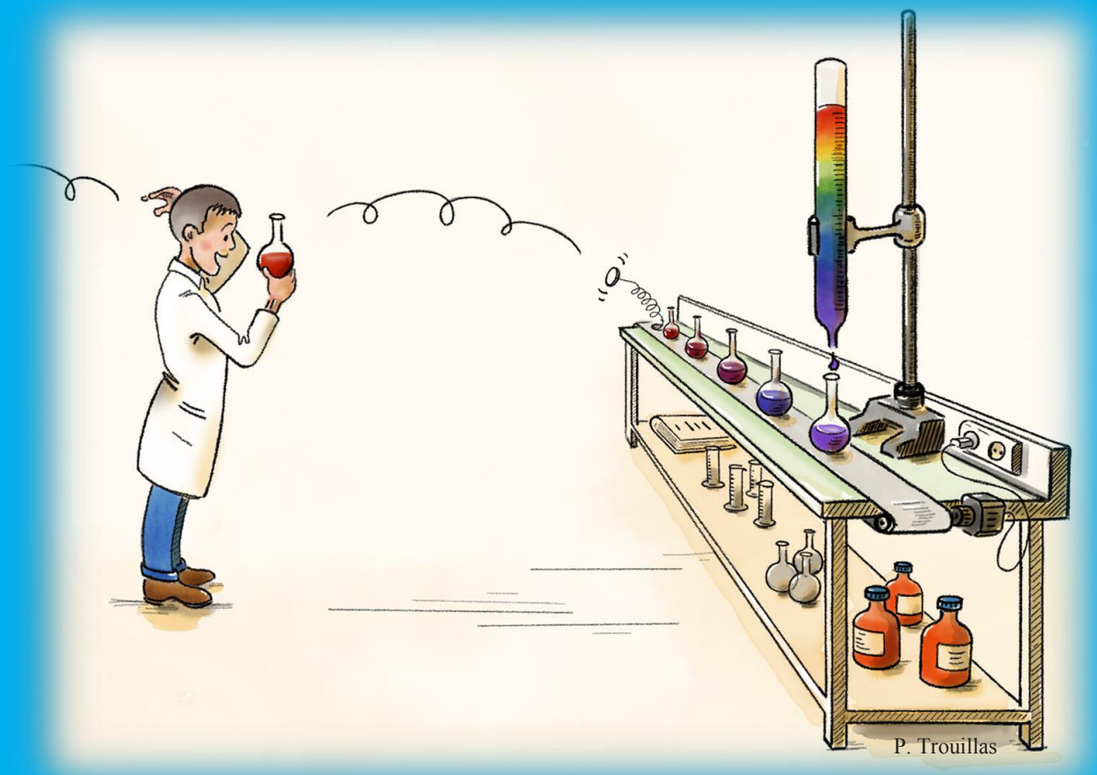

Dáire J. Gibbons

Triplet state access in multi-component heavy atom free photosensitizers in photomedicine

Dáire J. Gibbons

Cover design by Patrick Trouillas

ISBN: 978-94-6423-627-9
Digital version is available at http://dare.uva.nl

Printed and bound by ProefschriftMaken
Amsterdam, The Netherlands, 2021

Triplet state access in multi-component heavy atom free photosensitizers in photomedicine

ACADEMISCH PROEFSCHRIFT

ter verkrijging van de graad van doctor

aan de Universiteit van Amsterdam

op gezag van de Rector Magnificus

prof. dr. ir. K.I.J. Maex

ten overstaan van een door het College voor Promoties ingestelde commissie,

in het openbaar te verdedigen in de Aula der Universiteit

op vrijdag 28 januari 2022, te 11.00 uur

door Dáire John Gibbons

geboren te Dublin

Promotiecommissie

Promotores:	prof. dr. A.M. Brouwer	Universiteit van Amsterdam
	dr. S. Leroy-Lhez	Université de Limoges
Copromotores:	dr. R.M. Williams	Universiteit van Amsterdam
	dr. N. Villandier	Université de Limoges
Overige leden:	prof. dr. S. Woutersen	Universiteit van Amsterdam
	prof. dr. M.C.G. Aalders	Universiteit van Amsterdam
	prof. dr. H. Zhang	Universiteit van Amsterdam
	dr. F. Dumoulin	Acıbadem Mehmet Ali Aydınlar University
	prof. dr. S.A. Bonnet	Universiteit Leiden

Faculteit der Natuurwetenschappen, Wiskunde en Informatica

The research covered in this thesis was conducted within a Joint Doctorate in the Molecular Photonics Group at the Van 't Hoff Institute for Molecular Sciences, University of Amsterdam, in the PEREINE laboratoire, Université de Limoges, France and in the company PorphyChem in Dijon, France. The work was financially supported by the European Union's Horizon 2020 research and innovation programme under the Marie Sklodowska-Curie grant agreement no. 764837.

Table of contents

Table of contents i

1. Triplet states in multicomponent photosensitizers for photo-medicine 1

1.1. Introduction to Photodynamic Therapy 2

1.2. Advantages and Disadvantages of Photodynamic Therapy 5

1.2.1. Advantages of Photodynamic Therapy 5

1.2.2. Drawbacks of Photodynamic Therapy 7

1.3. Photochemistry of triplets in photosensitizers 8

1.4. Structural design of Photodynamic Therapy 12

1.4.1. Porphyrin-like molecules – Tetrapyrroles 12

1.4.2. Heptamethine cyanine dye 14

1.4.3. Lignin 15

1.4.4. Ideal photosensitizer for Photodynamic Therapy 17

1.4.4.1. Optical properties 18

1.4.4.2. Physicochemical properties 19

1.4.4.3. Targeting properties 20

1.5. Scope and outline of the thesis 21

2. Making Triplets from Photo-generated Charges: Observations, Mechanisms and Theory 33

2.1. Introduction 34

2.2. Fast Molecular Electron Donor-Acceptor systems (pre-2015) 36

2.3. BODIPY-based dimers and dyads 39

2.4. Polymer-Fullerene blends 51

2.5. Mechanistic aspects 56

2.6. Conclusions and Outlook 68

2.7. References 71

3. Photo-activated thin films of porphyrinoids for reactive oxygen species generation 77

3.1. Introduction 78

3.2. Results and Discussion 80

3.2.1. Synthesis and characterization 80

3.2.2. Photophysical characterization 81

3.2.2.1. Solution properties 81

3.2.2.2. Solid film properties 88

3.3. Conclusion 96

3.4. Experimental 96

3.4.1. Synthesis 96

3.4.2. Photophysical characterization in solution 97

3.4.3. Solid thin films 99

3.5. Supplementary Information 101

3.5.1. Synthesis and characterization 101

3.5.2. Photophysical characterization 105

3.5.2.1. Solution 105

3.5.2.2. Thin film 106

3.6. References 108

4. Lignin conjugates of porphyrins and cyanine dyes for biomedical applications 111

4.1. Introduction 112

4.2. Synthesis 114

4.2.1. Lignin-cyanine 114

4.2.2. Lignin-porphyrin 115

4.2.2.1. Tetra-carboxyphenylporphyrin (TCPP) 115

4.2.2.2. Mono-carboxyphenyl-triphenylporphyrin (m-CPTPP) 117

4.3. Photophysical studies 119

4.3.1. Lignin-cyanine conjugates 119
4.3.2. Lignin-porphyrin conjugates 124
4.3.2.1. TCPP 124
4.3.2.2. *m*-CPTPP 129
4.3.3. Lignin and acetylated lignin 132
4.4. Conclusion 133
4.5. Supplementary information 135
4.5.1. Experimental procedures 135
4.5.2. Supplemental spectra 138
4.5.3. Synthetic characterization 145
4.5.3.1. Lignin-cyanine synthetic characterization 145
4.5.3.2. TCPP-lignin synthetic characterization 148
4.5.3.3. *m*-CPTPP lignin conjugate 151
4.6. References 153
5. Free base porphyrin-cyanine conjugates for photomedicine 157
5.1. Introduction – Porphyrins and heptamethine cyanine dyes 158
5.2. Synthetic reaction schemes 160
5.3. Photophysical studies of the porphyrin-cyanine conjugate - TPPO-IR-783 161
5.3.1. UV-Vis spectroscopy 161
5.3.2. Photoluminescence – Fluorescence emission and singlet oxygen emission spectroscopy 165
5.3.3. Transient Absorption spectroscopy 174
5.4. Conclusion 177
5.5. Experimental procedures 179
5.5.1. Synthetic reaction schemes 179
5.5.2. Photophysical characterization 181

5.6. Supplementary information 182
5.7. References 188
6. Synthesis of photosensitizers for photomedicine 191
6.1. Introduction 192
6.1.1. Porphyrin-cyanine dye conjugates 192
6.1.2. Porphyrins in thin films 196
6.2. Discussion 197
6.2.1. Porphyrin-cyanine dye conjugates 197
6.2.2. Tetra-alkoxy-arylporphyrins 200
6.3. Conclusions 203
6.4. Synthetic experimental procedures 204
6.5. Experimental Spectra 210
6.6. References 222
7. Phenalenone-Triazolium Salt Derivatives for Antimicrobial Photodynamic Therapy 225
7.1. Introduction 226
7.2. Photophysical Results and Discussion 227
7.3. *In vitro* bacterial studies 232
7.4. Experimental section 236
7.5. References 239
Publications 241
Summary 243
Samenvatting 245
Resumé 249
Sommario 251
Acknowledgements 255

Photo-activated thin films of porphyrinoids for reactive oxygen species generation[‡]

Abstract

This chapter discusses the synthesis and photophysical studies, in both solution and thin film, of free base 5,10,15,20-tetra-(4-hexyloxyphenyl)porphyrin. The porphyrin was synthesized *via* modified Adler-Longo conditions. This porphyrin was then studied *via* UV-Vis spectroscopy, and steady-state and time-resolved photoluminescence spectroscopy. A thin film was cast on quartz glass *via* spin coating and *via* vapour-phase deposition. The fluorescence lifetime of the porphyrin in a solid film, as well as the detection of singlet oxygen generated by the film using a water-soluble singlet oxygen probe, are reported.

[‡]The content of this chapter has been submitted to the Journal of Porphyrins and phthalocyanines.

3.1. Introduction

The first written accounts of Photodynamic Therapy (PDT) were reported at the end of the 19th century.[1] Back then, it was coined as 'phototherapy'[2] and has since been developed to treat early stage tumors,[3] dermatological conditions[4] and microbial infections (Antimicrobial Photodynamic Therapy).[5] PDT requires the presence of molecular oxygen ($^3O_2$), a photosensitizer (PS) and light to form singlet oxygen ($^1O_2$) that is responsible for the desired therapeutic effect. The 'ideal PS' is highly sought after and its properties are described in reviews by Callaghan and Senge, and by Abrahamse and Hamblin (see also section **1.4.4**).[1, 6] Some of these properties include efficient triplet excited state formation with an excitation wavelength in the region of 650–850 nm (known as the therapeutic window), possessing a sufficiently long triplet lifetime, and generating high yields of singlet oxygen and Reactive Oxygen Species (ROS). Following irradiation of a PS, its singlet state is populated. This singlet state can then undergo intersystem crossing (ISC) to form the triplet state. The triplet state can interact with $^3O_2$ to form $^1O_2$ (Figure **3.1**), which can destroy cancer cells or microbial cells.

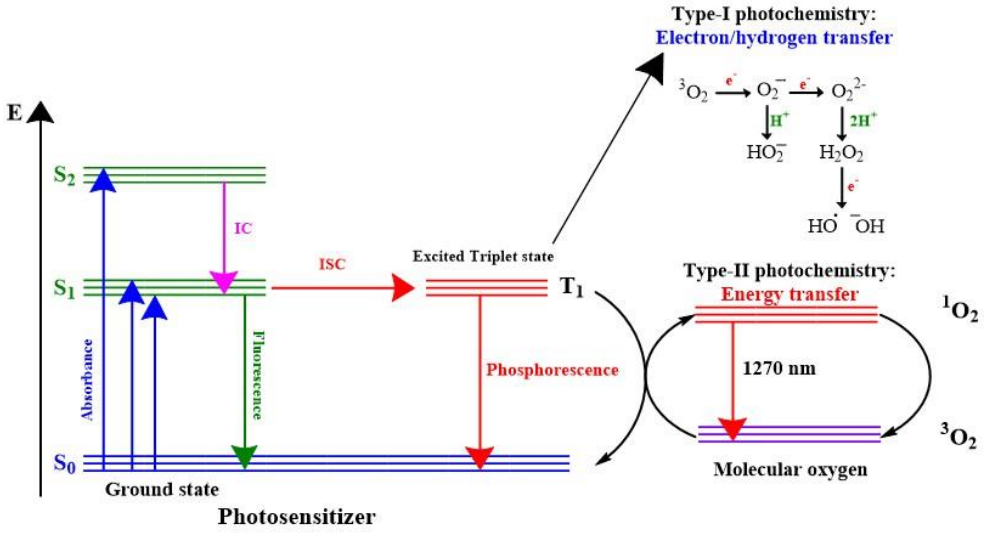

Figure 3.1. *Jablonski energy diagram showing how the photosensitizer is excited to the singlet state (S_1), followed by population of the excited triplet state by intersystem crossing (ISC) and the triplet state interacting with molecular oxygen to form cytotoxic singlet oxygen.*[7]

Antimicrobial Photodynamic Therapy (APDT) is the light treatment against harmful micro-organisms and has been applied in the clinics for almost thirty years.[8] It has been used to treat skin infections,[9] oral infections in dentistry[10] and more recently, it has been investigated as an alternative pest management in agriculture.[11] In order for the PSs to treat the microbial infections in the clinic, they have to be physically applied to the surface of the infected areas.

Furthermore, PSs have been incorporated into thin films for their uses as photodetectors and sensors.[12, 13]

The PS used in this study is the 5,10,15,20-tetra-(4-hexyloxyphenyl)porphyrin (**THOPP**), that was synthesized for the first time in 1993 by Shimizu *et al.*[14] It was recently shown that introducing a Zn(II) metal ion into the core of the **THOPP** macrocycle allowed an electroluminescence process to occur in thin films.[15] Furthermore, Shimizu and coworkers described the mesomorphic phase transitions of *meso*-tetra-(4-alkoxyphenyl)porphyrins with differing chain lengths.[14] **THOPP** appeared in numerous papers that reported on volumetric properties of porphyrins,[16] oxygen sensing,[17] fluorescence and FTIR analysis,[18] mesogenic properties of porphyrin liquid crystals,[19] and organic-inorganic surfaces in thin films.[20]

Since thin films containing *meso*-tetra-(4-alkoxyphenyl)porphyrins can exhibit luminescence,[15, 18] investigations were conducted to determine whether it is also possible to create singlet oxygen, *via* light excitation, in the thin film. Herein, the synthesis of a *meso*-tetra-(hexyloxyphenyl)porphyrin, **THOPP**, and its photophysical properties in solution, as well as in thin films, are described for application in photomedicine.

3.2. Results and Discussion

3.2.1. Synthesis and characterization

THOPP was synthesized (Figure **3.2**) *via* a modified literature procedure (see supplementary information for full synthetic procedure and characterization data - figures **S3.1**–**S3.6**).[15] The photophysical properties of **THOPP** were studied in solution and in a thin film. Results are summarized into tables **3.1**–**3.4** and commercially available 5,10,15,20-tetraphenylporphyrin (**TPP**) was used as a reference for properties in solution (see structure of **TPP** in Figure **3.2**).

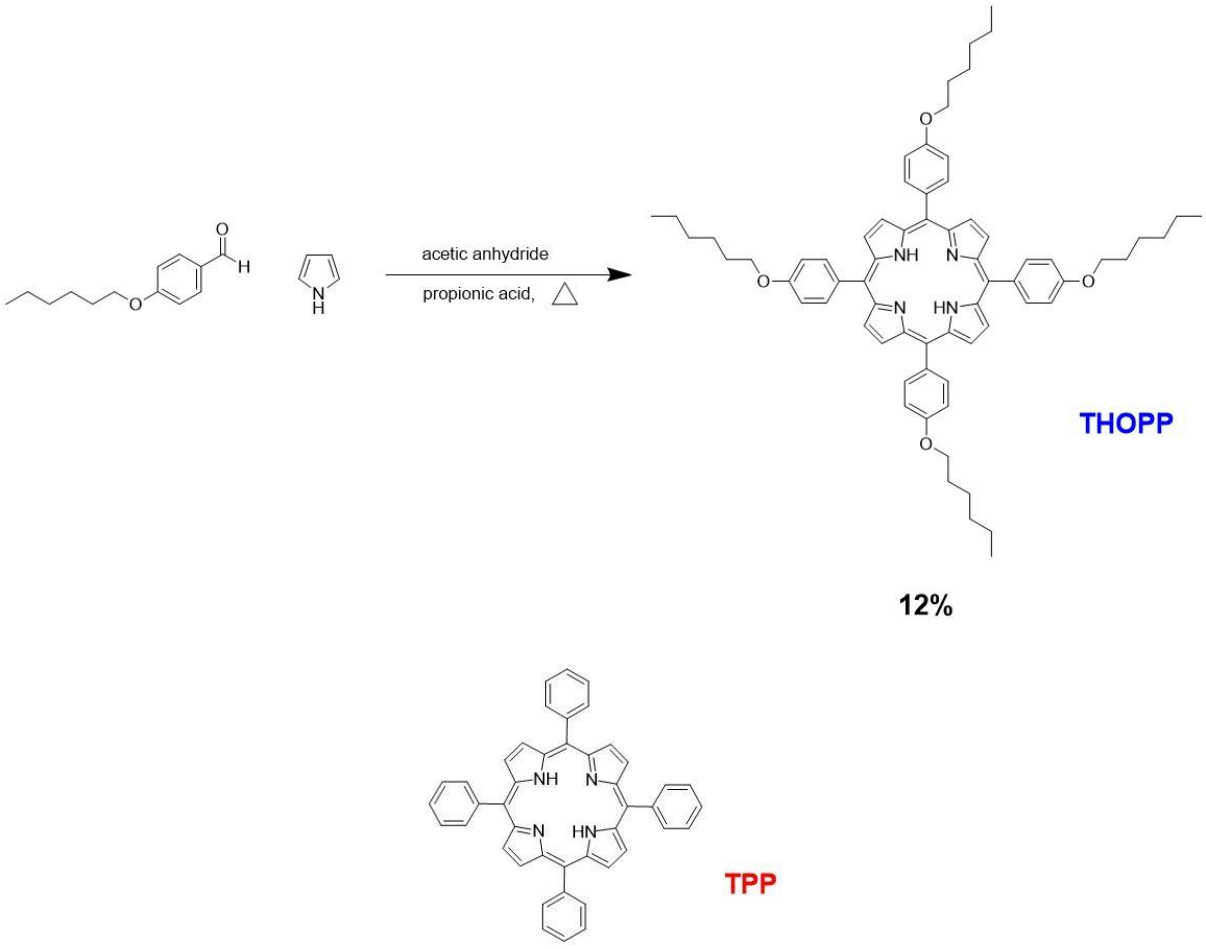

Figure 3.2. (Top): *Reaction scheme for the synthesis of 5,10,15,20-tetra-4-hexyloxyphenylporphyrin (**THOPP**) and **(Bottom):** chemical structure of 5,10,15,20-tetraphenylporphyrin (**TPP**).*[15]

3.2.2. Photophysical characterization

3.2.2.1. Solution properties

UV-Vis spectra of **THOPP** and **TPP** in chloroform ($CHCl_3$) (Figures **3.3** and **3.4**) are characteristic of free base porphyrins with an intense Soret band at 423 nm and 418 nm, respectively (Table **3.1**).[24, 30] These Soret bands both bear shoulders with maxima at 400 nm and four Q-bands (Q-band maxima are summarized in Table **3.1**). **THOPP** shows a small peak at 450 nm that corresponds to partial protonation of the porphyrin by the $CHCl_3$ solvent.[21] For this reason and for the determination of the triplet lifetime, **THOPP** was also studied in tetrahydrofuran (THF; see UV-Vis spectrum in Figure **S3.7**). Upon changing the solvent from $CHCl_3$ to THF, the Soret band shifts towards the blue region by 2 nm (see Table **3.1**). No partial protonation was observed, the Q-bands absorbed less light (as indicated by their reduced molar absorption coefficients), and they were shifted to the blue region by a max of 3 nm.

The UV-Vis spectrum of **TPP** in $CHCl_3$ also shows evidence of partial protonation by the acidity of the $CHCl_3$ solvent, as it has a small peak at approx. 440 nm. **THOPP** undergoes a bathochromic shift (4–9 nm) of all bands, compared to **TPP**. This is most likely due to the presence of electron-donating hexyloxy chains on the *para*-position of the phenyl rings. This structural difference therefore causes a shift towards the red region of the UV-Vis spectrum. The photoluminescence spectra were recorded in toluene and $CHCl_3$ to determine the fluorescence quantum yield (Φ_f) and the singlet oxygen quantum yield (Φ_Δ), respectively. In Figure **3.5**, it shows that the energy of the first excited state, S_1, of **THOPP** is 654 nm and 648 nm for **TPP**. The energy of the S_1 ($E(S_1)$) slightly lower for **THOPP** than for **TPP** and thus explains the bathochromic shift observed in the UV-Vis spectrum of **THOPP**, compared to **TPP**.

The concentration of **THOPP** in the UV-Vis spectrum was 2.3 μM (Figure **3.3**), while that of **TPP** in Figure **3.4** was 1.6 μM. Despite the higher concentration of **THOPP**, its Soret band absorbs less than **TPP** as shown by its lower molar absorption coefficient (Table **3.1** and in Figures **3.4** and **3.5**). However, the Q-bands of **THOPP** absorb more and their intensity ratio is different compared to **TPP** in $CHCl_3$. The intensity of these bands of **THOPP** in decreasing order, from longer to shorter wavelengths (low energy to high energy), are: $Q_{IV} > Q_{III} > Q_I > Q_{II}$. In **TPP**'s UV-Vis spectrum, the Q-bands decrease in order of: $Q_{IV} > Q_{III} > Q_{II} > Q_I$, with the Q_{IV}-peak much more intense than the others. This intense peak is followed by minor decreases in intensity from the Q_{III} to Q_I in the UV-Vis spectrum of TPP. However, **THOPP** shows a gradual decrease from Q_{IV} to Q_{III}, followed by a large decrease to the Q_{II}. Surprisingly,

the intensity almost doubles from the Q_{II} to Q_I in the UV-Vis spectrum of **THOPP**. These differences in the intensity ratio and position of the Q-bands are accredited to the molecular structure. Previous reports of **THOPP** show identical UV-Vis spectra, only differing slightly (Soret and Q-band experience shifts of 1–4 nm) due to the different solvents used.[17, 22]

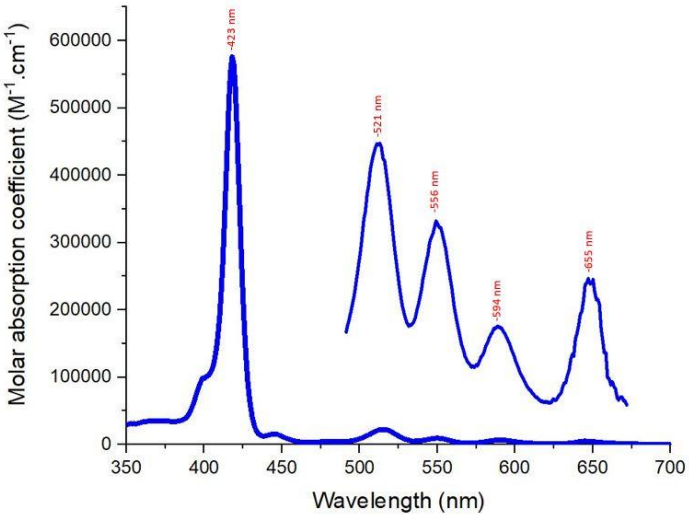

Figure 3.3. *UV-Vis spectrum of* ***THOPP****, in $CHCl_3$, using a molar absorption coefficient scale. The concentration of* ***THOPP*** *was 2.3 μM and the spectrum was recorded at room temperature.*

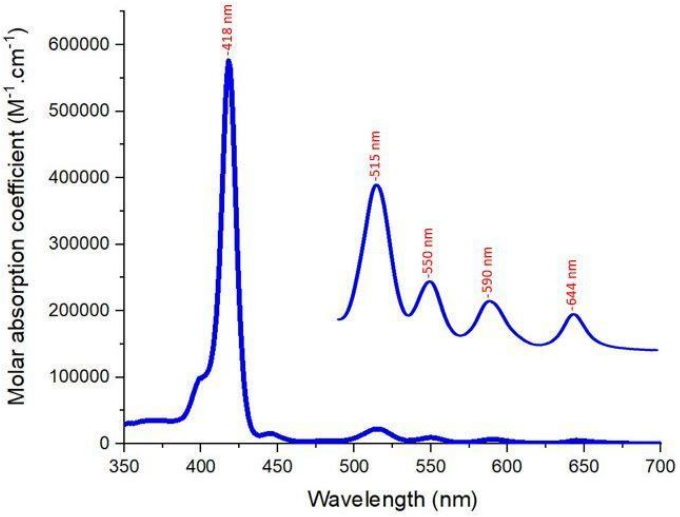

Figure 3.4. *UV-Vis spectrum of* ***TPP****, in $CHCl_3$, using a molar absorption coefficient scale. The concentration of* ***TPP*** *was 1.6 μM and the spectrum was recorded at room temperature.*

Table 3.1. *UV-Vis absorption data of the PSs,* ***THOPP*** *and* ***TPP****. The concentration was 2.3 μM for* ***THOPP*** *in $CHCl_3$, 2.2 μM for* ***THOPP*** *in THF, and 1.6 μM for* ***TPP*** *in $CHCl_3$. Values in brackets refer to the log of the molar absorption coefficient (ε).*

PS	Sh [a] (λ/nm)	Soret band (λ/nm)	Q-bands (λ/nm)				Q_y / Soret [b]
			Q_{IV} [c]	Q_{III} [d]	Q_{II} [e]	Q_I [f]	
THOPP – $CHCl_3$	400	423 (5.65)	521 (4.40)	556 (4.32)	594 (4.14)	655 (4.20)	0.02
THOPP - THF	400	421 (5.64)	518 (4.16)	554 (4.02)	596 (3.56)	654 (3.84)	0.02
TPP – $CHCl_3$	400	418 (5.76)	515 (4.35)	550 (3.97)	590 (3.82)	644 (3.69)	0.02

[a] Sh = shoulder that appears beside Soret band; [b] Ratio of the intensity of the Q_{III} band compared to the Soret band; [c] Q_{IV} = Qy(1,0) peak; [d] Q_{III} = Qy(0,0) peak; [e] Q_{II} = Qx(1,0) peak; [f] Q_I = Qx(0,0) peak.

The overlap of the absorption and emission spectra for **THOPP** and **TPP** in $CHCl_3$ are shown below. This overlap determines the experimental energy of the singlet excited state ($E(S_1)$; Figure **3.5**). This figure shows the wavelength at which the normalized absorption spectrum overlaps with the normalized emission spectrum. The $E(S_1)$ of **THOPP** in $CHCl_3$ is 654 nm and for **TPP** in $CHCl_3$, the $E(S_1)$ is 648 nm. This result is in close agreement with the literature value of 646 nm of **TPP**.[28]

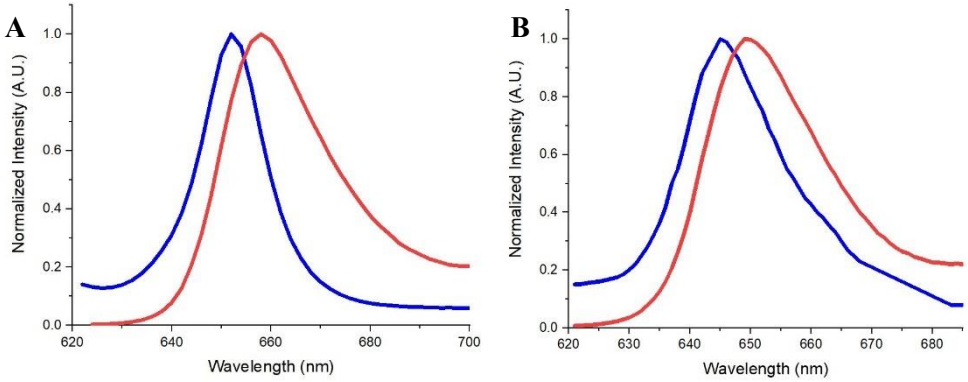

Figure 3.5. (A): THOPP's *normalized absorption (blue) and emission spectra (red) in $CHCl_3$. $E(S_1)$ of* ***THOPP*** *= 654 nm.* ***(B): TPP's*** *normalized absorption (blue) and emission spectra (red) in $CHCl_3$. $E(S_1)$ of* ***TPP*** *= 648 nm.*

Furthermore, the emission spectra of **THOPP** and **TPP** in $CHCl_3$ at room temperature are shown in Figure **3.6**. The emission maxima of **THOPP** appear at 655 nm and 725 nm. The former (Em1 as shown in Table **3.2**) is approximately three times more intense than the latter emission maximum (Em2). The fluorescence of **THOPP** in THF was also conducted (Figure **S3.8**). The position of the emission maxima, and the overall emission shape, remain unchanged

upon changing the solvent from $CHCl_3$ to THF. Furthermore, the Φ_f remains unchanged (Table **3.2**). **TPP** exhibits emission maxima at 649 nm and 718 nm in $CHCl_3$ (Figure **3.6**). All solutions (**TPP** in $CHCl_3$, and **THOPP** in $CHCl_3$ and THF) were excited at 518 nm and the absorbance at this wavelength was 0.1. **TPP**'s emission spectrum appears to have a more bimodal distribution shape as the Em1 emission band is almost 1.6 times more intense than the Em2 peak. **TPP**'s emission spectrum is overall less intense than **THOPP**. The **THOPP** emission profile reported here is slightly different compared to previous reports in the same solvent. Also, the Φ_f (**THOPP**) in this report is larger than previously reported (0.22 vs 0.13) by Şen *et al*.[18] and the τ_s reported herein is twice as long compared to that reported by Şen and coworkers.

Table 3.2. *Photophysical properties of* ***THOPP*** *in THF and* $CHCl_3$*, and* ***TPP*** *in* $CHCl_3$*.*

PS	Em1 [a] (nm)	Em2 [a] (nm)	SS [b] (cm^{-1})	Φ_f [c]	Φ_Δ [d]	τ_s (ns) [e]	τ_T (ns) [f]	τ_T (µs) [g]	
								τ1	τ2
THOPP – $CHCl_3$ [h]	655	725	70	0.22	0.44	- [i]	- [i]	- [i]	- [i]
THOPP – THF [j]	655	725	70	0.22	- [i]	9.4 ± 0.9	330 ± 4.5	297	46
TPP – $CHCl_3$ [h]	649 [h]	718 [h]	120 [h]	0.11 [h]	0.55 [h]	10.6 ± 0.3 [k]	480 [k]	385 [k]	*

*[a] According to the emission spectra, Em1 = first emission peak [λ_{em} $Q_x(0,0)$] and Em2 = second emission peak [λ_{em} $Q_x(0,1)$]; [b] The Stokes shift (SS) that was calculated from the corresponding UV-Vis and emission spectra; [c] Φ_f = fluorescence quantum yield calculated using TPP (0.11) as a reference in toluene;[24] [d] Φ_Δ = singlet oxygen quantum yield was calculated using TPP (0.55) as a reference in $CHCl_3$;[23] [e] τ_s = singlet state lifetime in air (equilibrated), given in nanoseconds; [f] τ_T (ns) = triplet state lifetime in air (equilibrated), given in nanoseconds; [g] τ_T (µs) = triplet state lifetime in oxygen-free solution (given in microseconds), the triplet state lifetime in the oxygen-free solution undergoes bi-exponential decay giving two lifetimes, τ1 and τ2, given in microseconds; [h] in $CHCl_3$ solvent; [i] data not available; [j] in THF solvent; [k] literature values in DMF solvent;[22] * no triplet-triplet annihilation reported in literature, it decays mono-exponentially, thus yielding one triplet lifetime.*

Figure **3.6** displays the fluorescence quantum yield (Φ_f) of **THOPP** in $CHCl_3$ and it was determined using **TPP** in toluene as a reference (0.11).[24] The fluorescence of **TPP** is lower than that of **THOPP** (Figure **3.6**). The Φ_Δ of **THOPP** in $CHCl_3$ was calculated using **TPP** in $CHCl_3$ as a reference (0.55).[23] The higher Φ_f in **THOPP** is compensated by the decreased singlet oxygen quantum yield of **THOPP** (0.44; Figure **3.7**). Therefore, the quantum yields confirm that intersystem crossing (ISC) in **TPP** is faster than in **THOPP**.

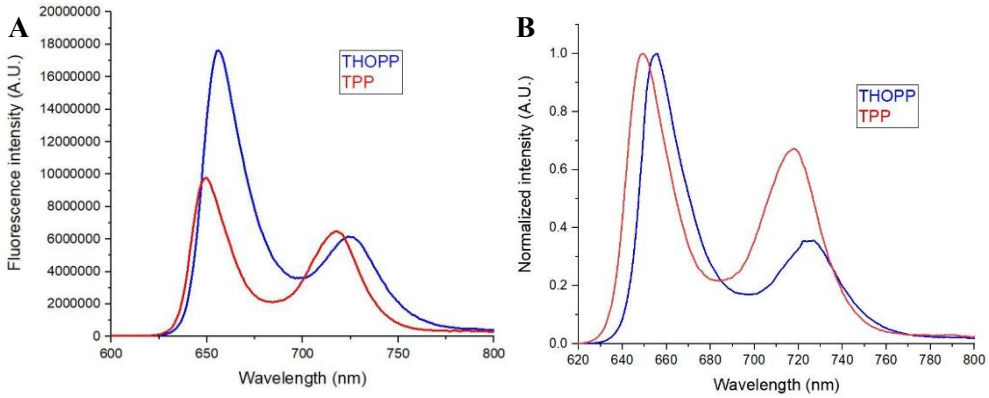

***Figure 3.6. (A)**: Fluorescence spectra of **THOPP** (blue) and **TPP** (red) in $CHCl_3$ using **TPP** in toluene (0.11) as a reference (Excitation wavelength = 518 nm and absorbance of both samples at this wavelength was 0.1).[24] The fluorescence quantum yield obtained for **THOPP** was 0.22. **(B)**: Normalized fluorescence emission spectra of **THOPP** (blue) and **TPP** (red) in $CHCl_3$.*

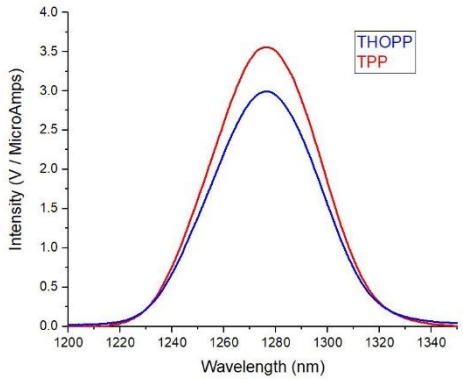

***Figure 3.7.** Singlet oxygen emission of **THOPP** (blue) and **TPP** (red) in $CHCl_3$ using **TPP** in $CHCl_3$ as a reference (0.55).[23] Excitation wavelength = 521 nm and the obtained singlet oxygen quantum yield was 0.44.*

In figure **3.8**, the nanosecond transient experiment of aerated **THOPP** in THF is reported. The experiment was first conducted in $CHCl_3$, however the sample decomposed after excitation by the pump laser (see experimental details). There was no decomposition observed in THF and the decay curve of this aerated sample is fitted mono-exponentially. The oxygen-free sample of **THOPP** in THF decays bi-exponentially (Table **3.2** and Figure **S3.9**). This indicates that triplet-triplet annihilation is predominantly occurring and this decay undergoes

second order decay kinetics. There is a slow and fast component observed and the slow component likely corresponds to the intrinsic lifetime of the triplet excited state of **THOPP** in oxygen-free THF (see section **3.5.1.1** for experimental details). The fast component would then correspond to triplet-triplet annihilation occurring (Table **3.2**). The lifetime of **TPP** in DMF was reported to be slightly longer than that of **THOPP** in THF (Table **3.2**).[22] This correlates well with the singlet oxygen quantum yield of **THOPP** (Figure **3.7**): the shorter triplet lifetime of **THOPP** produces a lower singlet oxygen yield.

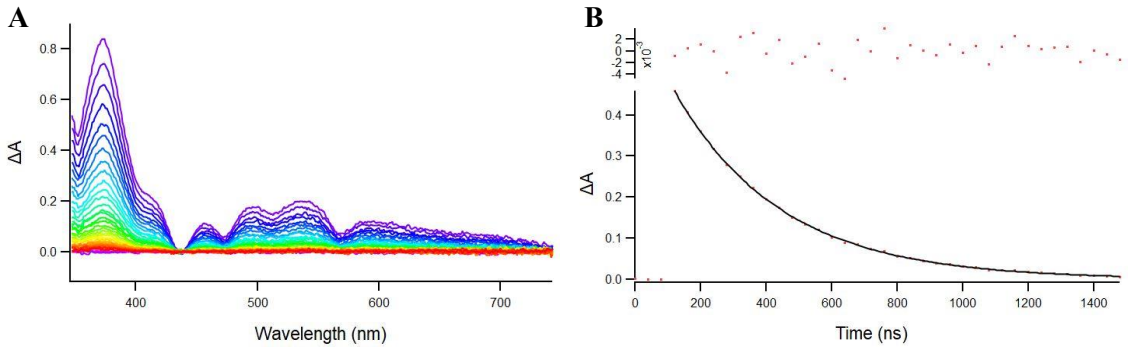

Figure 3.8. *(**A**): Nanosecond transient absorption spectrum of **THOPP** in THF (in air). λ_{ex} = 518 nm, incremental time delay = 40 ns. (**B**): Decay kinetics trace at 517 nm. Decay curve is fitted mono-exponentially and the obtained triplet lifetime is 330 ns. On the top, weighted residuals are presented.*

Table **3.2** reports a bi-exponential fit of the triplet decay data, however, a more appropriate model is second order decay kinetics. The observed triplet lifetime (T_1) is influenced by the triplet state being quenched by oxygen in solution, as well as by triplet-triplet annihilation (k_{TT}), and by the intrinsic triplet decay (k_0). Within the triplet-triplet annihilation process, the diffusion rate of the molecules in the triplet excited state, as well as their concentration at time zero (C_0; influenced by laser-power), plays an important role due to bimolecular collisional quenching.[25, 26]

The complex decay of triplet states and their interaction with oxygen also implies that singlet oxygen emission is due to a process with second order decay kinetics. This means that it can be fitted *via* a bi-exponential decay, as the concentration of the triplet at time 0 (C_0 in equations below) and the concentration of oxygen in solution, are of importance. The triplet decay can be fitted by a mono-exponential function if the interaction with oxygen is fast. Furthermore, it is clear that total removal of oxygen is not straightforward, indicated also by

the fact that the singlet oxygen emission quantum yield remained virtually the same upon prolonged bubbling with argon. These effects have also been noted by others.[37]

By using second order decay kinetics at room temperature in THF, we obtain an intrinsic triplet lifetime of τ^0_T = 566 µs, and a triplet-triplet annihilation rate constant of k_{TT} = 9.1 × 10^9 $M^{-1}s^{-1}$. This is close to the diffusion rate in THF, which is 1.3 × 10^{10} at 293 K. For pristine **C_{60}** in toluene[27] at room temperature, $\tau^0_T \geq$ 280 µs, with a $k_{TT} \geq$ 4.8 × 10^9 $M^{-1}s^{-1}$ was reported. The intrinsic triplet state lifetime τ^0_T of **TPP** is reported to be 1500 µs at 293 K.[28] This implies that the values reported here are within the range of expectation.

The (partly spectrally integrated) data vs time (t) was fitted with a home-made Igor procedure describing the following function:

$$\Delta A(t) = \frac{C_0 k_0}{k_0 e^{(k_0 t)} + k_{TT} C_0 (e^{(k_0 t)} - 1)}$$

Perhaps superfluous to note, this is mathematically equivalent to

$$\Delta A(t) = \frac{C_0 e^{-(k_0 t)}}{1 + C_0 (k_{TT}/k_0)(1 - e^{(k_0 t)})}$$

as well as

$$\Delta A(t) = \frac{C_0 k_0}{e^{(k_0 t)}(C_0 k_{TT} + k_0) - C_0 k_{TT}}$$

as used by others.[28, 29]

The concentration of the triplet excited state at time zero (C_0) was estimated by using the absorbance of the sample, the starting concentration, the excited volume (and depth) as well as the number of photons per pulse and was estimated to be 3.26 × 10^{-6} M. Based on the molar absorption coefficient of the triplet state of **TPP** at 790 nm of 6000 $M^{-1}cm^{-1}$, a concentration of triplet excited state at time zero (C_0) of 8.3 × 10^{-6} M was estimated. It has to be noted that the exact outcome of the fitting procedure is rather sensitive to the C_0 value, but within reasonable limits of the C_0 value (between 10% and an absolute maximum of 100% of the ground state concentration, 3.26 × 10^{-5} M). The variation of the outcome (of k_{TT}) is then a factor of ten.

Interestingly, and quite surprisingly, it has been reported that THF can react with singlet oxygen to form **THF-singlet oxygen adducts**.[29] Therefore, it is possible that the THF solvent slightly affects the triplet lifetime obtained. However, the reaction conditions reported in the paper by Sagadevan *et al*. show that these adducts are unlikely to form in our TA measurements. In particular, this paper reported reaction conditions of 2 hours irradiation with a blue LED light source (460 nm, 40 mW/cm^2). Our experiments were only 40 minutes in length with a pulsed laser (517 nm, 9 mW), which is too short for **THF-singlet oxygen adduct** formation.

The singlet excited state of **THOPP** decays mono-exponentially in THF (Figure **3.9**). This S_1 lifetime is 9.33 ns and is almost 6 times longer than the Zn(II) derivative of this compound (1.51 ns in THF).[15] However, the freebase of **THOPP** has a slightly shorter S_1 lifetime than **TPP** in DMF (10.6 ns).[22] The reduced S_1 lifetime is due to the increased rate of ISC associated with the Zn(II) in the macrocycle. Thus, the competitive relationship between fluorescence to the ground state and intersystem crossing to the triplet state, from the singlet excited state, is evident here.

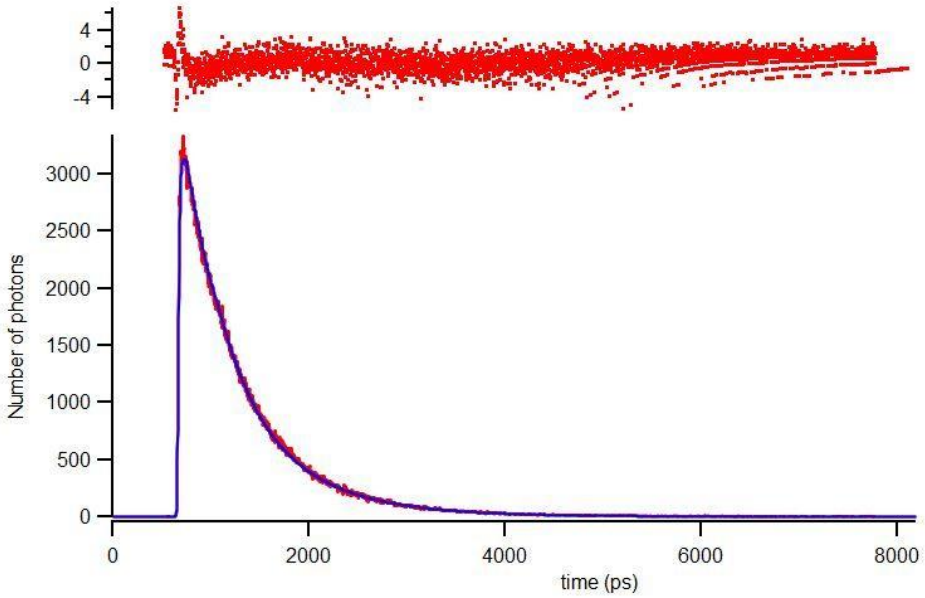

Figure 3.9. *Time-correlated single photon counting (TC-SPC) spectrum of* ***THOPP*** *in THF. Excitation wavelength = 560 nm. Emission wavelength = 650 nm. The absorbance was 0.05 at the excitation wavelength. Laser power is 0.44 mW and at this power,* ***THOPP*** *decayed mono-exponentially, the S_1 lifetime is 9.33 ns. On the top, weighted residuals are presented.*

.

3.2.2.2. Solid film properties

THOPP in THF (10 mg mL^{-1}) was spin coated to make a thin film on quartz glass. The UV-Vis spectrum was recorded (Figure **3.10**) and the data is summarized in Table **3.3**.

Film UV-Vis spectra

Some differences were observed between the UV-Vis spectra of **THOPP** in solution and in the film. The major difference observed in the thin film spectrum (Figure **3.10**) is a large 19 nm shift of the Soret band in the thin film to the near-IR regions (Table **3.3**). Other small deviations are seen in the positions of the Q-bands with the largest difference observed in the Q_{II} band (hypsochromic shift of 5 nm). In terms of band characteristics, the Q-bands of **THOPP** in the film are approximately the same width as in solution (approximately 40 nm for Q_{IV}). Furthermore, there is a higher Q_{III} to Soret band ratio in the film compared to solution (Q_{III} / Soret = 0.12 vs 0.02).

Compared to the **Zn(II)THOPP** in a thin film,[15] there are four Q-bands in the free base porphyrin film due to the absence of a metal in the core (2 Q-bands), which is known to occur because of symmetry.[30] The Soret band in the Zn(II) species is slightly blue-shifted (438 nm) compared to the free-base counterparts (440 nm), with the Q-bands of the Zn(II) species appear at 560 nm and 602 nm.[15]

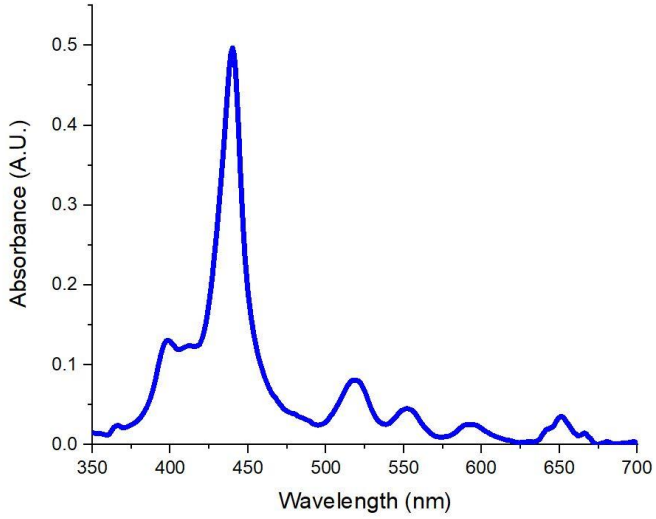

Figure 3.10. *UV-Vis spectrum of* ***THOPP*** *thin film spin coated onto quartz glass.*

Table 3.3. *UV-Vis absorption data of* ***THOPP*** *in a thin film obtained via spin coating.*

PS	Soret band (λ/nm)	Sh [a] (λ/nm)	Q-bands (λ/nm)				Q_y / Soret [b]
			Q_{IV} [c]	Q_{III} [d]	Q_{II} [e]	Q_I [f]	
THOPP	440	400	519	551	591	651	0.12

[a] Sh = shoulder that appears beside Soret band; [b] ratio of the intensities of the $Q_y(0,0)$ and Soret band of the porphyrin in the film; [c] $Q_{IV} = Q_y(1,0)$ peak; [d] $Q_{III} = Q_y(0,0)$ peak; [e] $Q_{II} = Q_x(1,0)$ peak; [f] $Q_I = Q_x(0,0)$ peak.

The excitation wavelength used for the emission spectrum of the **THOPP** thin film is 440 nm and the porphyrin emission is visible in the 600–800 nm region approximately (as seen in figure **3.11**). Interestingly, there is a sharp emission peak that arises at 741 nm which does not appear in solution. This peak most likely appears due to the presence of J-aggregates in the film.[31, 32, 33] The presence of aromatic groups at the *meso* positions in porphyrins has been reported to cause the formation of J-aggregates.[34, 35] The peak, at 741 nm, can be removed by making thin films *via* vapour-phase deposition (see Figure **3.15**). It is generally more intense than the Em2 peak. There is almost no Stokes shift in the film compared to the solution and this differs in the Zn(II) species,[27] where there is the presence of a meaningful Stokes shift. In a **THOPP** solution, there is a presence of a monomeric form in the emission spectrum. Whereas this "aggregation" peak in the emission spectrum of the **THOPP** film, suggests that the porphyrin forms J-aggregates in the film.

Table 3.4 *Photophysical properties of* ***THOPP*** *thin films obtained by spin coating (SC) and vapour-phase deposition (VP).*

PS	Em1 [a]	Em2 [a]	Em3 [b]	SS (cm^{-1}) [c]	S_1 lifetime (ns) [d]			
					Full power [e]		Half power [e]	
					τ1 (Amp) [f]	τ2 (Amp) [f]	τ1 (Amp) [f]	τ2 (Amp) [f]
THOPP SC	651	719	741	0	0.745 (0.51)	0.239 (0.49)	0.749 (0.42)	0.368 (0.58)
THOPP VP	648	714	- [g]	0	- [h]	- [h]	- [h]	- [h]

[a] According to the emission spectra, Em1 = first emission peak [λ_{em} $Q_x(0,0)$] and Em2 = second emission peak [λ_{em} $Q_x(0,1)$], Excitation wavelength = 440 nm and emission was measured in nm; [b] Em3 = peak that appears at 741 nm that is due to the formation of a J-aggregate in the film; [c] SS = The Stokes shift was calculated from the corresponding UV-Vis and emission spectra; [d] The film of ***THOPP*** *undergoes a bi-exponential decay at both full and half power, due to singlet-singlet annihilation, see Figure* ***3.12****; [e] The laser power was changed from full power to half power and it was measured as 0.44 mW and 0.22 mW, respectively; [f] Amp. = amplitude associated with values for bi-exponential fitting. [g] No J-aggregate in THOPP film achieved by vapour-phase deposition (VP); [h] No data available.*

Emission spectra of films

Figure **3.11** shows the emission spectrum of **THOPP** on a quartz film that was obtained *via* spin coating. The emission is similar to that observed in solution, however there is a large peak at 741 nm that is due to the formation of J-aggregates in the thin film (see below).

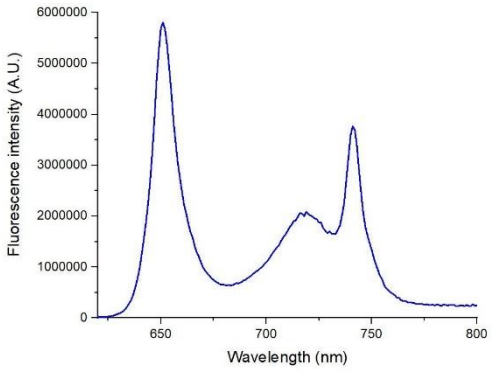

Figure 3.11. *Emission spectrum of spin coated* ***THOPP*** *thin film on quartz glass. Excitation wavelength= 440 nm.*

Porphyrin aggregation: J-band emission

The sharp features of the new emission band (at 741 nm) in the films are reminiscent of J-band emission.[34] In fact, a very similar emission band has been attributed to such phenomenon before for TPPS type molecules,[35, 36] as well as other porphyrins[37, 38, 39] and ZnTPP.[40]

Fluorescence lifetime determination using time-correlated single photon counting (TC-SPC)

Figure **3.12** shows the fits of the S_1 decay kinetics of **THOPP** in THF, and in a thin film at full laser power and half laser power (0.44 mW and 0.22 mW, respectively). The S_1 decay spectra in solution is shown above (Figure **3.9**) and that of the film at both full and half power are in the SI (Figures **S3.10** and **S3.11**).

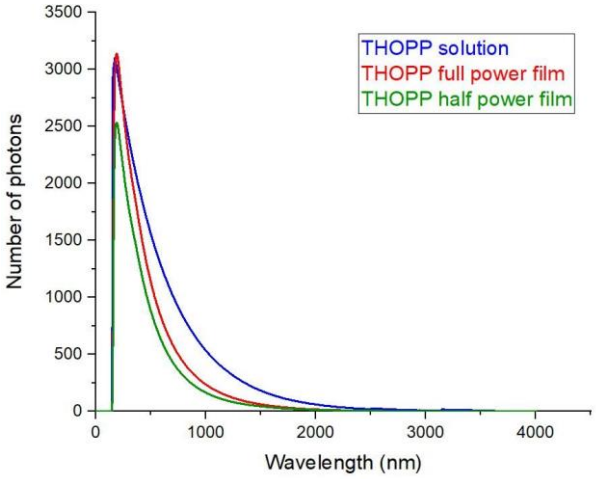

Figure 3.12. *Time-correlated single photon counting (TC-SPC) fitted spectrum of* ***THOPP*** *in THF solution (blue) and a thin film, at a full laser power (red) and half laser power (green). Excitation wavelength = 560 nm. Emission wavelength = 650 nm. The absorbance was 0.05 at the excitation wavelength for all species. Full power includes the laser power being at 0.44 mW while at half power, the laser power is 0.22 mW.*

THOPP in solution has a much longer S_1 lifetime than in the film, as clearly shown above as it decays slower than that of the film (Figure **3.12**). Within the film, the laser power does not appear to have much effect on the lifetime (Table **3**.**4**). Intuitively, the τ_2 is longer in the half-power (approx. 0.1 ns longer) as the weaker laser power causes depopulation of the S_1 state at a slower rate. In the thin film, the singlet decays *via* bi-exponential decay kinetics in both laser power conditions applied (100% and 50%). The lifetime of **THOPP** at full laser power (0.44 mW) in the film is 0.745 ns. Reducing the laser power to half power (0.22 mW) yields a S_1 lifetime of 0.749 ns. The second lifetime obtained from the bi-exponential fitting is likely due to singlet-singlet annihilation. To our knowledge, this is the first reported fluorescence lifetime of this porphyrin in a solid thin film.

Porphyrin film: Singlet oxygen detection

In order to measure the singlet oxygen production of **THOPP** in a solid film, a solvent or medium is needed to detect the singlet oxygen generated. The main reason for this is that the emission intensity of singlet oxygen depends on its steady state concentration present in a particular solvent.[41] In the above spectra and discussion (Figures **3.10**–**3.12**), the UV-Vis and emission spectra are conducted in air. Attempts were conducted to measure singlet oxygen emission in air using these films (obtained *via* spin coating), however there was no signal detected. Moreover, even though the singlet oxygen lifetime is sufficiently long in organic

solvents,[42] it was found that the porphyrin thin films obtained by spin coating dissolves in organic solvents. Thus, an aqueous solvent, a reliable method to detect singlet oxygen, and films that are stable in aqueous media, were needed.

A water-soluble singlet oxygen probe called AquaSpark, that has an emission maximum at 515 nm, is an ideal candidate (see mechanism of emission in figure **3.13**).[43]

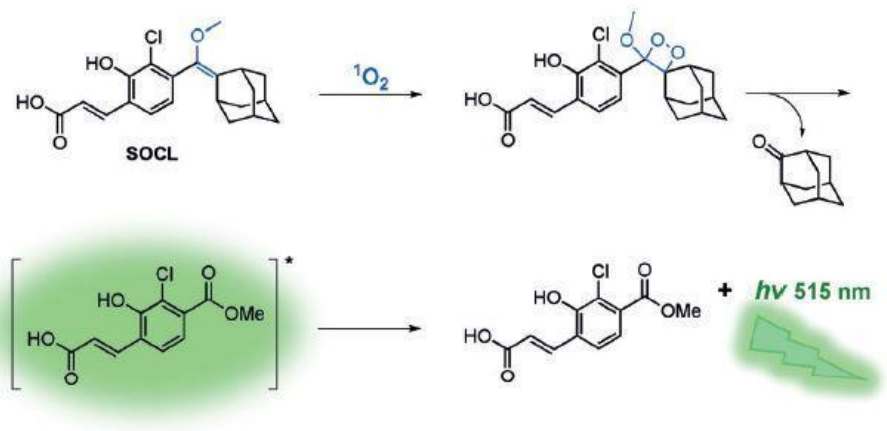

Figure 3.13. *Mechanism of AquaSpark probe (**SOCL**) reacting with singlet oxygen to give emission at 515 nm.*[43]

This probe has been shown to be selective towards singlet oxygen compared to other reactive oxygen species.[43] New films, that are stable in aqueous media, were made using a modified vapour-phase deposition technique (see experimental section: solid thin films for protocol) and its photophysical properties were determined. The UV-Vis spectrum of this new film is shown below (Figure **3**.**14**) and the data is summarized in Table **3**.**5**.

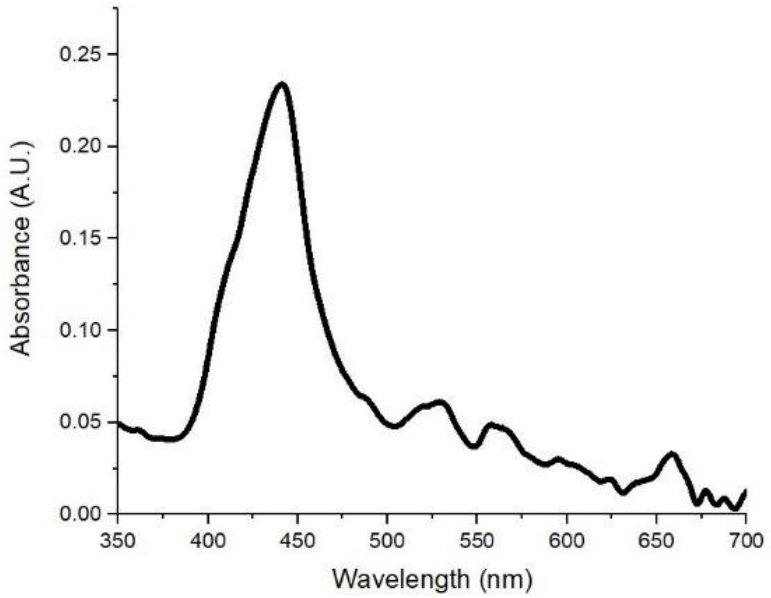

Figure 3.14. *UV-Vis spectrum of* ***THOPP*** *thin film on quartz glass made by vapour-phase deposition.*

Table 3.5. *UV-Vis absorption data of* ***THOPP*** *in a thin film obtained via vapour-phase deposition.*

PS	Soret band (λ/nm)	Q-bands (λ/nm)				Q_y / Soret [a]
		Q_{IV} [b]	Q_{III} [c]	Q_{II} [d]	Q_I [e]	
THOPP	440	528	556	601	661	0.15

[a] *Ratio of the intensity of the $Q_y(0,0)$ band compared to the Soret band;* [b] *$Q_{IV} = Q_y(1,0)$ peak;* [c] *$Q_{III} = Q_y(0,0)$ peak;* [d] *$Q_{II} = Q_x(1,0)$ peak;* [e] *$Q_I = Q_x(0,0)$ peak.*

From the UV-Vis spectrum of the thin film made by vapour-phase deposition, there is a profile similar to that observed in solution and in the films made by spin coating (see figures **3.3** and **3**.**10**). The spectrum has the characteristics of a porphyrin: a large Soret band and four small Q-bands. The Q-bands are visible and compared to the spin coated thin film, the Soret band is less intense compared to the Q-bands and all of the peaks appear to be red-shifted by at least 5 nm. This newly formed film was excited with 418 nm light and an emission spectrum was recorded (see figure **3.15**). Compared to the films made by spin coating, there is no J-band observed in these films (peak at 741 nm). Clearly, J-aggregates are formed during the spin coating process, but not *via* the vapour-phase deposition technique.

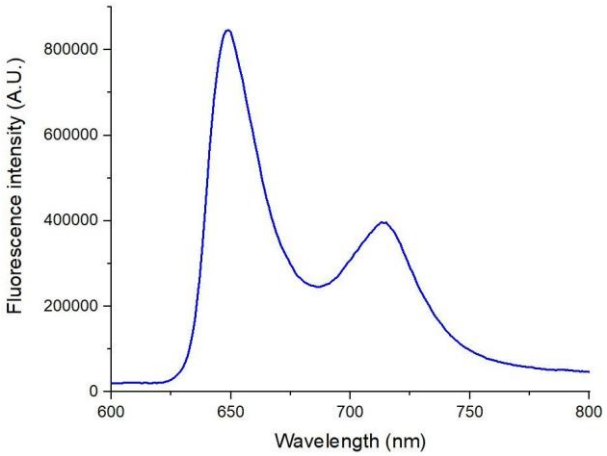

Figure 3.15. *Emission spectrum of a* ***THOPP*** *thin film on quartz glass made by vapour-phase deposition. Excitation wavelength = 418 nm.*

Table 3.6. *Emission data of a* ***THOPP*** *thin film obtained via vapour-phase deposition.*

PS	Em1 [a]	Em2 [a]
THOPP	648	714

[a] *According to the emission spectra, Em1 = first emission peak [λ_{em} $Q_x(0,0)$] and Em2 = second emission peak [λ_{em} $Q_x(0,1)$], Excitation wavelength = 418 nm.*

The **THOPP** thin film was placed in a large cuvette containing the AquaSpark solution and an emission spectrum was obtained (see figure **3.16**).

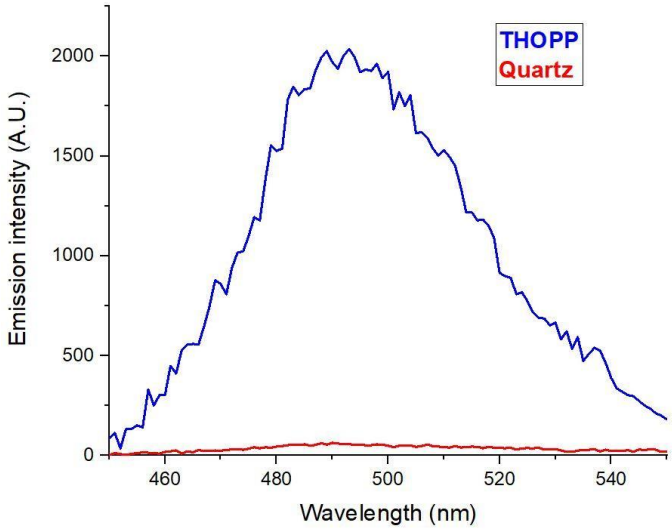

Figure 3.16. *Singlet oxygen detection via AquaSpark probe after exciting the* ***THOPP*** *PS in a thin film. The reference is a quartz plate in AquaSpark probe solution. Excitation wavelength = 650 nm.*

This showed that the **THOPP** photosensitizer (PS), even in a thin film, is capable of producing singlet oxygen. The only difference between the **THOPP** thin film and the quartz plate was the presence of the PS. The excitation wavelength used was 650 nm. This was chosen as the production of singlet oxygen *via* near IR light is highly sought after for photo medical applications. The near IR light can penetrate deep into the human tissue to activate the PS in the thin film that can be present on an implant and produce $^1O_2$ for antimicrobial effects.

3.3. Conclusion

THOPP was synthesized, and its photophysical properties were determined in solution, using **TPP** as a reference. While **THOPP** produces a slightly smaller amount of singlet oxygen compared to **TPP** (0.44 and 0.55 in $CHCl_3$, respectively), a novel approach to apply **THOPP** as a photosensitizer is to include it in a thin film. Due to its long alkyl tails, the film formation is improved. The fluorescence emission and lifetimes in the film are a lot shorter than in solution and the reported fluorescence lifetime of **THOPP** in a film, as well as its singlet oxygen emission, are reported herein. The future potential impact of this is that the water-resistant **THOPP** thin film can be activated using near IR light. The near IR light can penetrate deep within human tissue to produce singlet oxygen that can kill cancer or bacteria in the body. This can be envisaged as a novel way to clean an implant: **THOPP** can produce the singlet oxygen that would kill the bacteria that are accumulating at the implant.

3.4. Experimental

The synthesis was carried out in the laboratories of Porphychem, Dijon, France.

3.4.1. Synthesis[15]

4-Hexyloxybenzaldehyde (5.00 mL, 4.96 g, 24.04 mmol, 1.00 eq.), 2.6 ml freshly distilled pyrrole (2.60 mL, 2.51 g, 37.48 mmol, 1.56 eq.) and 1 mL acetic anhydride was dissolved in 100 mL propionic acid. The reaction mixture was stirred under reflux conditions at 130°C for 4 hours. The reaction mixture was cooled slowly to room temperature. The reaction mixture was then filtered and the filtrate was washed with methanol. The crude product was then recrystallized using a 1:1 $CHCl_3$:MeOH mixture and the product was filtered. The product was washed with methanol and allowed to dry overnight to obtain a crystalline purple solid (**1.17 g**, **12% yield**). ^{1}H NMR (500 MHz, $CDCl_3$): δ -2.73 (s, 2 H, 2 x NH), 1.00 (t, 12 H, 4 x CH_3),

1.48 (m, 16 H, 8 x CH_2), 1.64 (m. 8 H, 4 x CH_2), 1.97 (m, 8 H, 4 x CH_2), 4.23 (t, 8 H, 4 x CH_2), 7.29 (d, 8 H, 8 x Ar-H), 8.11 (d, 8 H, 8 x Ar-H), 8.85 (s, 8 H, 8 x Ar-H) ppm. ^{13}C NMR (600 MHz, $CDCl_3$): δ13.14, 22.72, 25.94, 29.50, 31.75, 68.35, 112.71, 119.82, 134.48, 135.61, 158.98 ppm. UV-Vis (THF) λ_{max} (log ε) (ε, mM^{-1} cm^{-1}): 421 (438.5), 518 (13.4), 552 (9.3), 597 (1.4), 652 (13.6). HRMS (MALDI): Calcd for $C_{82}H_{75}N_6NaO_7S_2$: *m/z* 1342.3713 ($[M]^+$). Found: *m/z* 1015.518 ($[M]^+$).

3.4.2. Photophysical characterization in solution

Materials and techniques

The photophysical characterization was conducted in $CHCl_3$ and THF (spectroscopy grade, supplier = Merck).

Absorption and photoluminescence spectra

Both UV-Vis absorption spectra and fluorescence emission spectra were recorded at 21ºC. UV-Vis absorption spectra were measured in quartz cuvettes (1 cm path-length, Hellma) using a HP/Agilent 8453 UV-Vis and Shimadzu UV2700 spectrophotometer. Fluorescence emission spectra were recorded on a SPEX Fluorolog 3 fluorometer. In this fluorometer, double grating monochromators are used in the excitation and emission channels. A Xenon arc lamp (450 W, Osram) is the excitation light source, and a Peltier cooled photomultiplier tube (R636-10, Hamamatsu) is the detector. The fluorescence signal from the fluorophores in solution is collected in a right-angle geometry, and the fluorescence spectra are corrected for fluctuations of the excitation source flux and for the wavelength dependence of the detection sensitivity. The absorbance for photoluminescence spectra was approximately 0.1 for solution.

Fluorescence and Singlet Oxygen Quantum yields

Both quantum yields were determined using the SPEX fluorolog 3 fluorometer relative to a fluorescent/singlet oxygen standard of a known quantum yield. From here, the integrated emission spectra of the unknown sample are compared with that of the standard under the same absorbance conditions (absorbance = 0.1) at the same excitation wavelength. The integrated emission spectra are corrected for the skewed baselines where appropriate.

For these measurements, dilute solutions with absorbances of approximately 0.1 at one of the Q-bands in the absorption spectrum were used. Absorption and emission spectra (both fluorescence and singlet oxygen) were measured using 3.0 ml of the sample and standard solutions in 1 x 1 cm optical path length quartz cells. The quantum yields were calculated using the equation **3.1** [44] below:

$$Q_x = Q_r[A_r(\lambda_r)/A_x(\lambda_x)][I(\lambda_r)/I(\lambda_x)][(n_x)^2/(n_r)^2](D_x/D_r) \quad \textbf{(Equation 3.1)}$$

Where Q_x = the desired quantum yield (fluorescence or singlet oxygen) of the unknown sample; Q_r = the (fluorescence of singlet oxygen) quantum yield of the known sample according to literature; $A_r(\lambda_r)$ = absorbance of the reference at the excitation wavelength; $A_x(\lambda_x)$ = absorbance of the unknown sample at the excitation wavelength; $I(\lambda_r)$ = relative intensity of the exciting light of a known reference at wavelength λ; $I(\lambda_x)$ = relative intensity of the exciting light of an unknown sample at wavelength λ; n_x = refractive index of the solvent that the unknown sample is dissolved in; n_r = refractive index of the solvent that the known sample is dissolved in; D_x = integrated area under the corrected emission spectrum of the unknown sample; D_r = integrated area under the corrected emission spectrum of the known sample. In both cases, the integrated area was corrected for the skewed baseline (if present), thereby lowering the area under the emission curve. The data was analyzed using the Origin program and excel.[45] **Note:** For singlet oxygen measurements, the unknown and reference sample must be in the same solvent.

Nanosecond transient absorption spectra

Triplet state lifetimes were determined by means of nanosecond time-resolved absorption spectroscopy using an EKSPLA NT342B laser system in which the third harmonic of a Nd:YAG laser system (355 nm) was used to pump an OPO (to give λ_{ex} = 517 nm, pulse width which has an adjustable gate width of minimal 2.9 ns and laser power range of 1–3 mJ per pulse). This setup is described in full detail in the literature.[46] The data was analyzed using Igor 7 Pro (Wavemetrics, Lake Oswego, OR, USA).[47] The absorbances of the solutions used were approximately 0.5. For the oxygen-free solution, the solution was bubbled with argon for 1–2 hours prior to laser excitation *via* this setup.

Time correlated single photon counting spectra

Time-resolved emission measurements were performed on a picosecond single photon counting setup. The excitation wavelength (560 nm) is generated by the output of a fully automatic tunable Ti:sapphire laser (Chameleon Ultra, Coherent). This source produces a sub-picosecond excitation pulse, (full-width half-maximum, FWHM). The repetition rate is decreased from the fundamental 80 MHz to a lower value (usually 8 MHz) using a pulse picker (Pulse Select, APE). After second harmonic generation (SHG), a dichroic mirror is used to separate the doubled light which is directed to the sample. Fundamental light is guided *via* a delay line to a fast photodiode (PD) and used as a reference pulse. The emission is collected at a 'magic angle' (54.7^o) and focused onto a multichannel plate photomultiplier tube (MCP-PMT, R3809U-50, Hamamatsu) through a single-grating monochromator (Newport Cornerstone 260, f=250mm, grating 300ln/mm blaze 422 or grating 300ln/m blaze 750nmM20, Carl Zeiss, 600 lines/mm). Although the excitation source produces sub-picosecond pulses, the electronics and the detector cause a broadening of the signal and are the limiting factor of the time resolution. The overall instrument response function (IRF) was 20 ps (FWHM) for the

solution of the measured compound, which is measured from a dilute scattering solution (Ludox) at the excitation wavelength.

3.4.3. Solid thin films

Precleaning

Three square quartz glass slides (see provider and description below) were washed with a brush, soap and water in a beaker. The slides were then placed into a Teflon substrate holder using forceps. The glass slides in the substrate holder were submerged in deionized water before sonication for 15 minutes. The water was then replaced by acetone and the beaker was further sonicated for 15 minutes. The acetone was replaced by isopropanol and further sonicated for 15 minutes. The glass slides were allowed to dry. Compressed air was used to accelerate the drying process. The glass slides were then placed back into the substrate holder and were placed inside a UV-ozone photoreactor for 30 minutes.

Provider and description of thin films

Provider: Präzisions Glas & Optik GmbH;

Description: 2.5 x 2.5 cm^2 quartz glass substrates with a thickness of 1.1 mm - CNC precision-cut, no bevel.

Spin coating procedure for thin film formation

Three quartz glass slides were cleaned with the precleaning technique as described above. Almost immediately after being removed from the UV-ozone photoreactor, the slides were then mounted on the spin coating machine, (Delta 10, Ble Laboratory Equipment GmbH). The vacuum was switched on to approximately 0.6 bar. The spin speed, spinning time and acceleration settings were set. 10 mg/ml **THOPP** samples were prepared, sonicated and filtered into a sample vial. They would then be drawn into a syringe (0.3 ml) per slide. They would then be spun to form films.

Vapour-phase deposition procedure for thin film formation

Three glass slides were cleaned with the precleaning technique as described above. Almost immediately after being removed from the UV-ozone photoreactor, 10 mg of the **THOPP** porphyrin was then placed at the bottom of a 100 ml two-neck round bottom flask. A slide was then carefully placed to be over the porphyrin solid. The flask was carefully attached to a Schlenk line and the pressure of the system inside the flask was reduced to 10^{-4} mbar. The solid was then heated slowly from 250^{o}C to 400^{o}C using a heat gun or until the solid had been vaporized and formed a layer on the slide. The slide was then allowed to cool to room temperature to create a water stable thin film.

Absorption and photoluminescence spectra of thin films

Both UV-Vis absorption spectra and fluorescence emission spectra were recorded at 21°C and on a thin film support. The instruments were then used as described in section **3.4.2**.

Time correlated single photon counting of a thin film

The time-resolved emission measurements were performed as described above in section **3.4.2**. The differences were that the film was placed on a thin film support and the overall instrument response function (IRF) was 8 ps (FWHM) for the thin film.

AquaSpark™ 515 Singlet Oxygen Probe

This singlet oxygen probe was supplied by Carbosynth and a 50 ml 2 μM AquaSpark PBS solution was made. For measuring singlet oxygen, the excitation wavelength used was 650 nm and emission was observed from 450 nm to 550 nm, using the same settings as the fluorescence emission spectra. The film was placed into a large cuvette (20 ml capacity) and the THOPP film was excited in the presence of the AquaSpark probe. A quartz slide was used as a reference.

3.5. Supplementary Information

3.5.1. Synthesis and characterization

The porphyrin, 5,10,15,20-tetra-(4-hexyloxyphenyl)porphyrin (**THOPP**), was synthesized according to the protocol described in 3.4.1.[15]

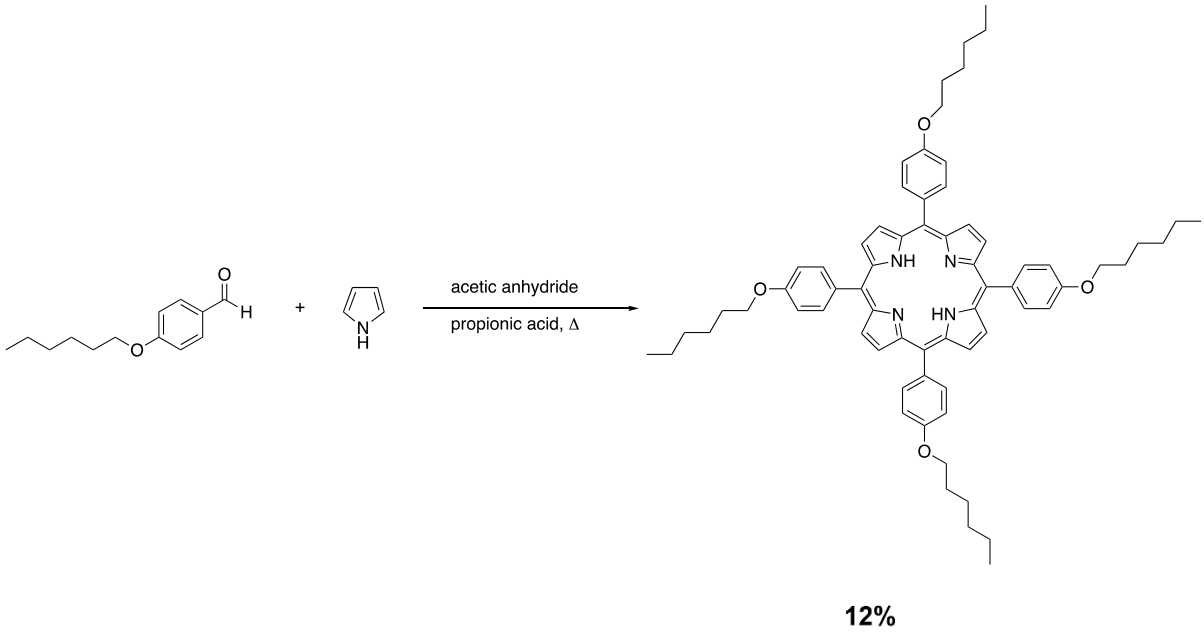

Figure S3.1. *Reaction scheme of 5,10,15,20-tetra-(4-hexyloxyphenyl)porphyrin (**THOPP**).*[15]

Synthesis of THOPP and characterization

The synthesis of this A_4 *meso*-substituted porphyrin was in a slightly lower yield, compared to literature.[15] This can be explained by the large increase in scale of the reaction and **THOPP** was fully characterized using ^{1}H and ^{13}C NMR, Mass spectroscopy, UV-Vis Spectroscopy and HPLC (Figures **S3.2**–**S3.6)**. The ^{1}H NMR spectrum (Figure **S3.1**) is pure according to literature.[15] The only difference is at the peak 1.64 ppm, there are 12 protons instead of 8 and this is likely due to the water in the humid atmosphere. There is another small peak at around 2.2 ppm. The ^{13}C spectrum (Figure **S3.3**) is out of phase and cannot be fully corrected however it is not that significant. There are two carbons missing from the spectrum: the alpha- and beta-carbon in the pyrrole moieties of the porphyrin macrocycle. This has also been reported in the literuature.[15] The β carbons have been reported for this compound, however though the peak is very broad and has a low intensity.

The MALDI TOF mass spectrum of **THOPP** (Figure **S3.4**) shows two peaks at: 1015 ($M+H^+$) and 226 (HABA matrix). In figure **S3.5**, the $M+H^+$ peak is the most intense and it has been previously reported that mass peaks of M+6 occur in porphyrins.[48]

The HPLC analysis shows that there are no impurities in the product. There were no other peaks present apart from that shown in Figure **S3.6**. The product was dissolved in $CHCl_3$ and injected into the HPLC normal phase column (stationary phase = SiO_2 and mobile phase = $CHCl_3$) to determine purity. The elution time of the product was 2.94 minutes. There were no products or impurities that eluted off during HPLC indicating the product is 99.9% pure.

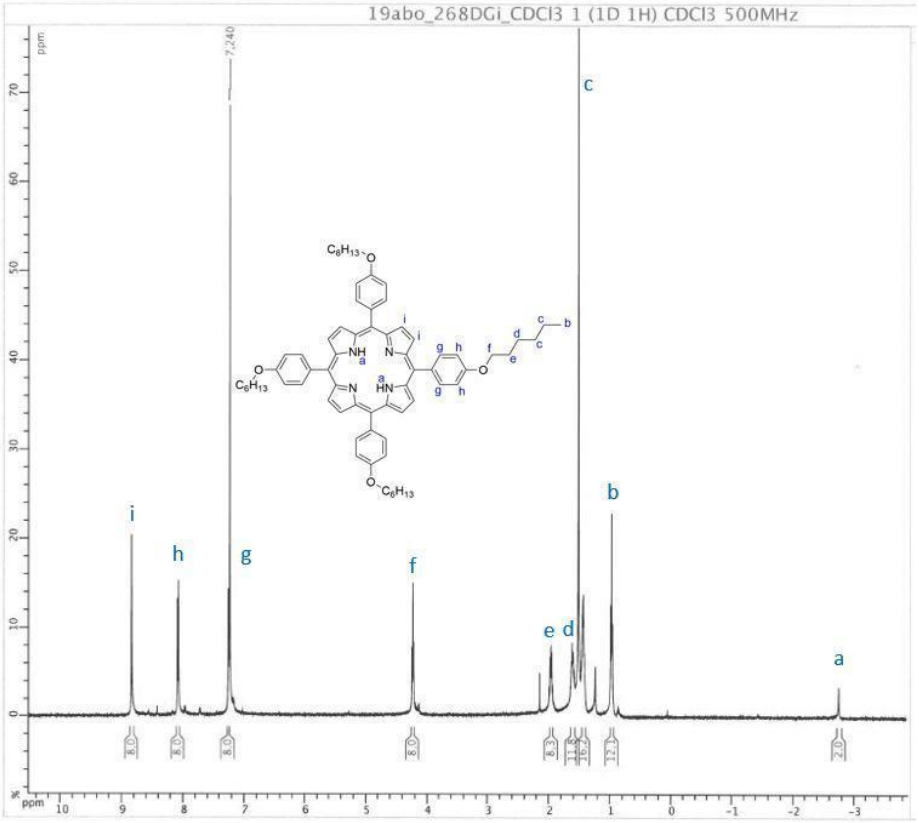

Figure S3.2. *Fully integrated ^1H NMR spectrum of* ***THOPP****, dissolved in deuterated chloroform ($CDCl_3$), with the structure and the labels for the protons in the structure.*

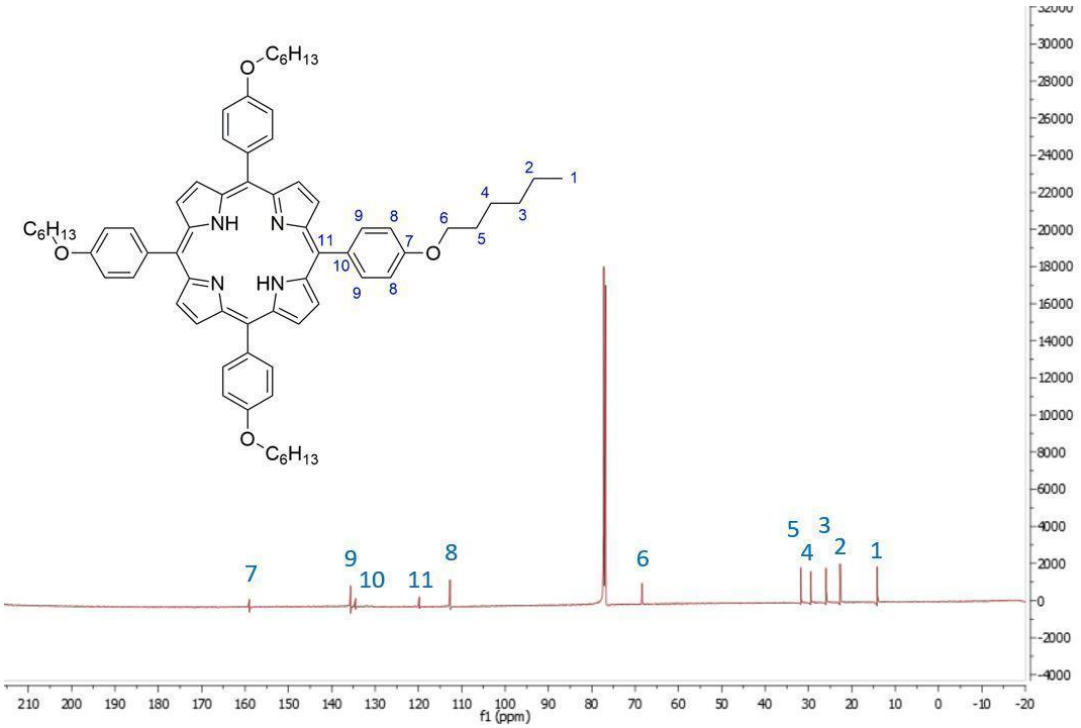

Figure S3.3. *^{13}C NMR spectrum of **THOPP**, dissolved in deuterated chloroform ($CDCl_3$), with the structure and the labels for the carbons in the structure.*

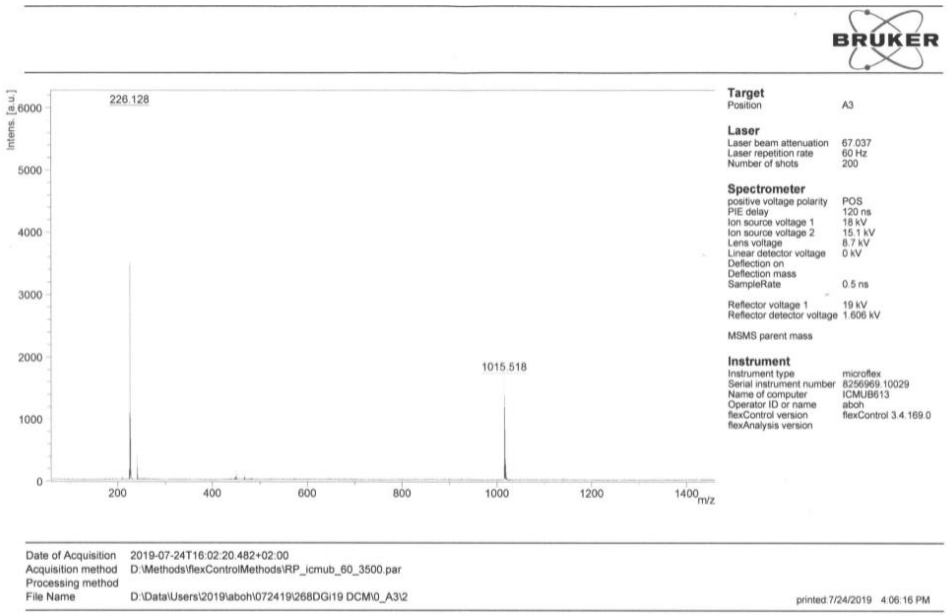

Figure S3.4. *Mass spectrum of **THOPP** using MALDI-TOF dissolved in dichloromethane (CH_2Cl_2).*

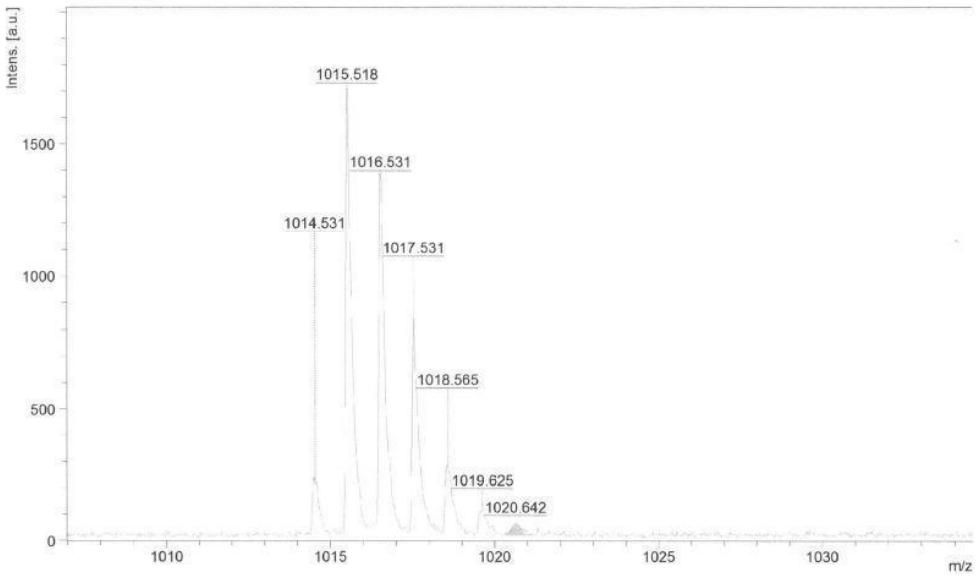

Figure S3.5. *Mass spectrum zoom, using MALDI-TOF displaying the isotope pattern of* ***THOPP****, dissolved in dichloromethane (CH_2Cl_2).*

Chromatogram and Result:

Injection Details

Injection Name:	**268DGi19**	*Run Time (min):*	**10.00**
Vial Number:	**GE2**	*Injection Volume:*	**10.00**
Injection Type:	**Unknown**	*Channel:*	**UV_VIS_2**
Calibration Level:		*Wavelength:*	**420**
Instrument Method:	**Standard_CHCl3_modified**	*Bandwidth:*	**4**
Processing Method:	**Standard Processing Method**	*Dilution Factor:*	**1.0000**
Injection Date/Time:	**25/juil./19 16:00**	*Sample Weight:*	**1.0000**

Chromatogram

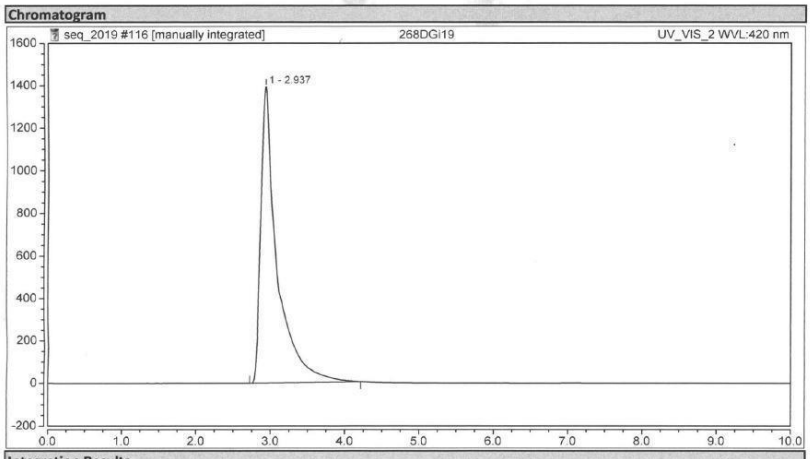

Integration Results

No.	Peak Name	Retention Time min	Area mAU*min	Height mAU	Relative Area %	Relative Height %	Amount n.a.
1		2.937	353.045	1394.164	100.00	100.00	n.a.
Total:			**353.045**	**1394.164**	**100.00**	**100.00**	

Figure S3.6. *HPLC analysis of* ***THOPP*** *using normal stationary phase silica column, dissolved in $CHCl_3$.*

3.5.2. Photophysical characterization

3.5.2.1. Solution

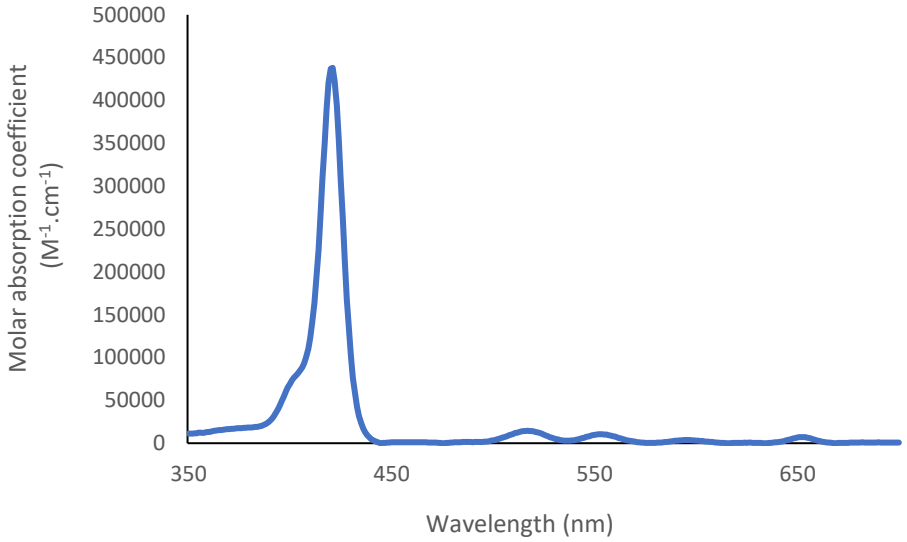

Figure S3.7. *UV-Vis spectrum of* ***THOPP*** *at room temperature, dissolved in THF. The concentration of THOPP in the THF solution was 2.2 µM. The y axis is a molar absorption coefficient scale.*

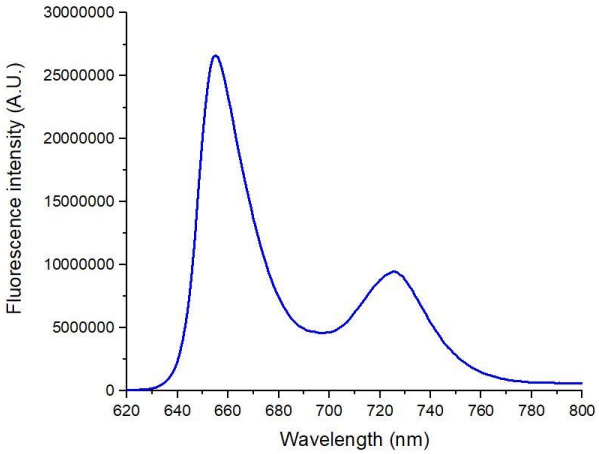

Figure S3.8. *Emission spectrum of* ***THOPP*** *at room temperature in THF, after excitation at 518 nm. The absorbance of the solution at 518 nm was 0.1.*

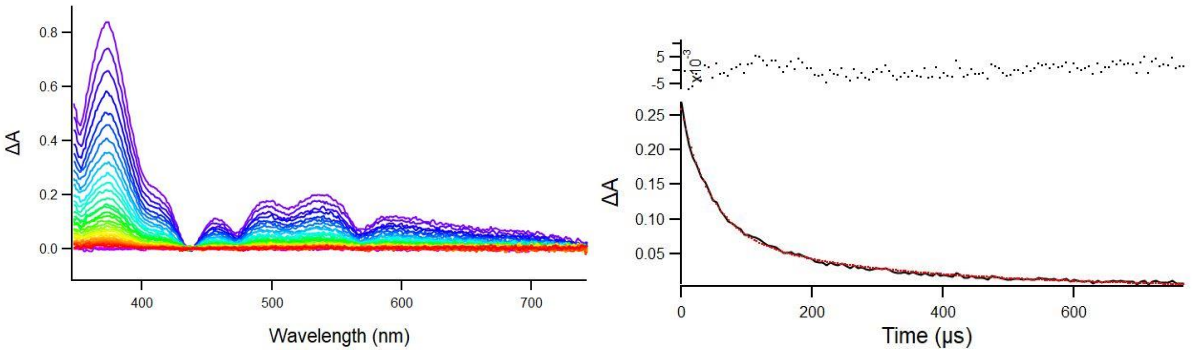

Figure S3.9. *(Left): Nanosecond transient absorption spectrum of* ***THOPP*** *in THF (in oxygen-free solution). Excitation wavelength = 517 nm, incremental time delay = 6 μs. (Right): Decay kinetics trace at 517 nm. The decay curve was decayed bi-exponentially and the obtained triplet lifetime was 297 ± 30 μs. On the top, weighted residuals are presented.*

3.5.2.2. Thin film

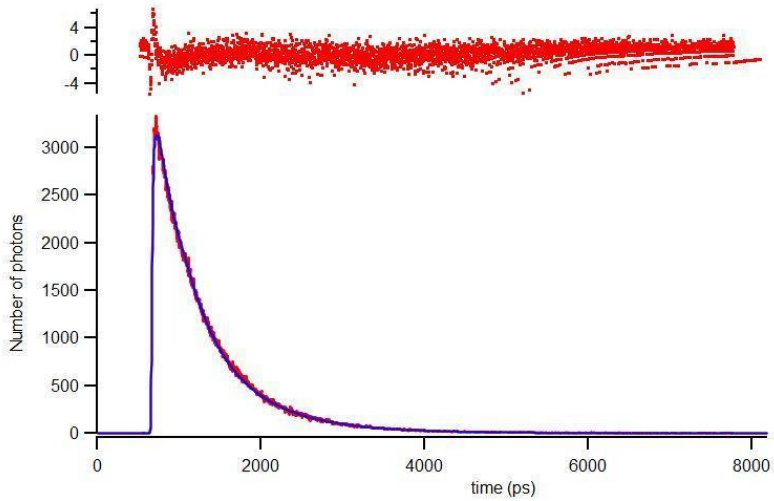

Figure S3.10. *Time-correlated single photon counting spectrum of* ***THOPP*** *in a thin film (at full laser power). Excitation wavelength = 560 nm. Emission wavelength = 650 nm. The absorbance was 0.05 at the excitation wavelength (560 nm). Laser power is 0.44 mW and* ***THOPP*** *decays bi-exponentially in this film at this laser power. The S_1 lifetime in these conditions is 0.745 ns. On the top, weighted residuals are presented.*

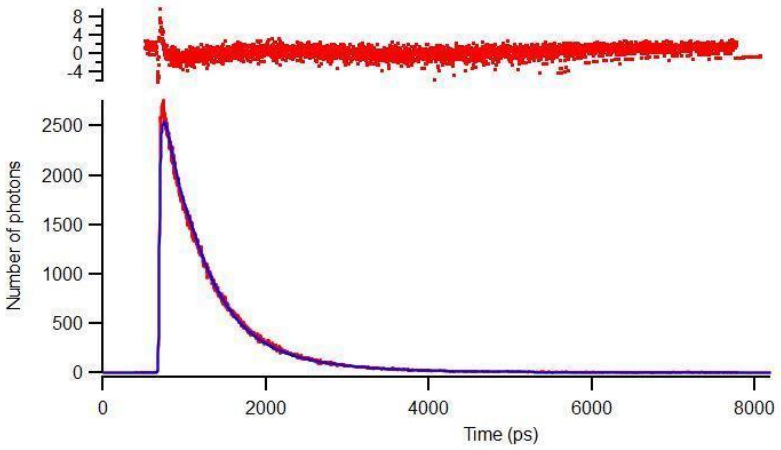

Figure S3.11. *Time-correlated single photon counting spectrum of* ***THOPP*** *in a thin film (at half laser power). Excitation wavelength = 560 nm. Emission wavelength = 650 nm. The absorbance was 0.05 at the excitation wavelength (560 nm). Laser power is 0.22 mW and* ***THOPP*** *decays bi-exponentially in this film at this laser power. The* S_1 *lifetime in these conditions is 0.749 ns. On the top, weighted residuals are presented.*

3.6. References

[1] S. Callaghan and M. O. Senge, The good, the bad and the ugly – controlling singlet oxygen through design of photosensitizers and delivery systems for photodynamic therapy, *Photochem. Photobiol. Sci.,* 2018, **17**, 1490–1514. doi: 10.1039/C8PP00008E

[2] N. R. Finsen, La Photothérapie, Georges Carré et C. Naud, 1899, Paris.

[3] P. Agostinis, K. Berg, K. A. Cengel, T. H. Foster, A. W. Girotti, S. O. Gollnick, S. M. Hahn, M. R. Hamblin, A. Juzeniene, D. Kessel, M. Korbelik, J. Moan, P. Mroz, D. Nowis, J. Piette, B. C. Wilson and J. Golab, Photodynamic Therapy Of Cancer: An Update, *CA Cancer J. Clin*., 2011, **61**, 250–281. doi: 10.3322/caac.20114.

[4] K. Kalka, H. Merk and H. Mukhtar, Photodynamic therapy in dermatology, *J. Am. Acad. Dermatol*., 2000, **42**, 389–413. doi: 10.1016/s0190-9622(00)90209-3

[5] M. Wainwright, Photoantimicrobials and PACT: what's in an abbreviation?, *Photochem. Photobiol. Sci*., 2019, **18**, 12–14. doi: 10.1039/C8PP00390D

[6] H. Abrahamse and M. R. Hamblin, New photosensitizers for photodynamic therapy, *Biochem. J*., 2016, **473**, 347–364. doi: 10.1042/BJ20150942

[7] J. M. Dąbrowski, B. Pucelik, A. Regiel-Futyra, M. Brindell, O. Mazuryk, A. Kyzioł, G. Stochel, W. Macyk and L. G. Arnaut, Engineering of relevant photodynamic processes through structural modifications of metallotetrapyrrolic photosensitizers, *Coord. Chem. Rev.*, 2016, **325**, 67–101. doi: 10.1016/j.ccr.2016.06.007

[8] F. Cieplik, D. Deng, W. Crielaard, W. Buchalla, E. Hellwig, A. Al-Ahmad and T. Maisch, Antimicrobial Photodynamic Therapy – What We Know and What We Don't, *Crit. Rev. Microbiol.,* 2018, **44**, 571–589. doi: 10.1080/1040841X.2018.1467876.

[9] M. Wainwright, The Problem with Dyes in Infection Control, *Dyes Pigm.,* 2017, **146**, 402–407. doi: 10.1016/j.dyepig.2017.07.042.

[10] H. Gursoy, C. Ozcakir-Tomruk, J. Tanalp and S. Yilmaz, Photodynamic Therapy in Dentistry: A Literature Review, *Clin. Oral Investig.,* 2013, **17**, 1113–1125. doi: 10.1007/s00784-012-0845-7.

[11] V. Ambrosini, M. Issawi, V. Sol and C. Riou, Photodynamic Inactivation of Botrytis Cinerea by an Anionic Porphyrin: An Alternative Pest Management of Grapevine, *Sci. Rep.,* 2020, **10**, 17438. doi: 10.1038/s41598-020-74427-9.

[12] A. W. Utari, B. Purnama and K. Abraha, Utilization of Natural Porphyrin Thin Films as a Photosensitizer for Photodetectors, *Adv. Mater. Res.*, 2014, **896**, 187–191. doi: 10.4028/www.scientific.net/AMR.896.187.

[13] B. Long, O. Bakr and F. Stellacci, Reversible Aggregation of Porphyrins in the Solid State, *J. Exp. Nanosci.,* 2008, **3**, 53–60. doi: 10.1080/17458080802073091.

[14] Y. Shimizu, M. Miya, A. Nagata, K. Ohta, I. Yamamoto and S. Kusabayashi, Mesomorphic phase transitions of tetraphenylporphyrins with four long aliphatic chains, *Liq. Cryst*., 1993, **14**, 795–805. doi: 10.1080/02678299308027756

[15] A. Charisiadis, A. Bagaki, E. Fresta, K. T. Weber, G. Charalambidis, C. Stangel, A. G. Hatzidimitriou, P. A. Angaridis, A. G. Coutsolelos and R. D. Costa, Peripheral Substitution of Tetraphenyl Porphyrins: Fine-Tuning Self-Assembly for Enhanced Electroluminescence, *ChemPlusChem*., 2017, **82**, 1–13. doi: 10.1002/cplu.201700416

[16] W. Zielenkiewicz, G. L. Perlovich, G. E. Nikitina and O. A. Golubchikov, Volumetric Properties of Methyl, tert-Butyl, and Alkoxy Derivatives of Tetraphenylporphyrin in Benzene Solution, *J. Solution Chem.*, 1997, **26**, 633–679. doi: 10.1007/BF02767620

[17] S. Z. Topal, M. Z. Ongu, E. Önal, K. Ertekin and C. Hirel, Hyperporphyrin effect on oxygen sensitivity of free meso-tetraphenylporphyrins, *Dyes Pigm.*, 2017, **144**, 102–109. doi: 10.1016/j.dyepig.2017.05.022

[18] P. Şen, C. Hirel, C. Andraud, C. Aronica, Y. Bretonnière, A. Mohammed, H. Ågren, B. Minaev, V. Minaeva, G. Baryshnikov, H. -H. Lee, J. Duboisset and M. Lindgren, Fluorescence and FTIR Spectra Analysis of Trans-A2B2-Substituted Di- and Tetra-Phenyl Porphyrins, *Materials,* 2010, **3**, 4446–4475. doi: 10.3390/ma3084446

[19] P. Bhyrappa, C. Arunkumara, B. Varghesea, D. S. S. Rao and S. K. Prasad, Synthesis and mesogenic properties of β-tetrabrominated tetraalkyloxyporphyrins, *J. Porphyr. Phthalocyanines*, 2008, **12**, 54–64. doi: 10.1142/S108842460800008X

[20] N. Minamijima, N. Furuta, S. Wakunami and T. Mizutani, Functionalization of Silica Surface by Tetrahydroxyporphyrin via SiO Linkages, *Bull. Chem. Soc. Jpn*., 2011, **84**, 794–801. doi: 10.1246/bcsj.20100317

[21] T. Bruhn and C. Brückner, The Origin of the Absorption Spectra of Porphyrin N- and Dithiaporphyrin S-Oxides in Their Neutral and Protonated States, *Phys. Chem. Chem. Phys.,* 2015, **17**, 3560–3569. doi: 10.1039/C4CP04675G

[22] B. Röder, M. Büchner, I. Rückmann and M. O. Senge, Correlation of photophysical parameters with macrocycle distortion in porphyrins with graded degree of saddle distortion, *Photochem. Photobiol. Sci*., 2010, **9**, 1152–1158. doi: 10.1039/C0PP00107D

[23] L. M. Mazur, T. Roland, S. Leroy-Lhez, V. Sol, M. Samoc, I. D.W. Samuel and K. Matczyszyn, Efficient Singlet Oxygen Photogeneration by Zinc Porphyrin Dimers upon One- and Two-Photon Excitation, *J. Phys. Chem*., 2019, **123**, 4271–4277. doi: 10.1021/acs.jpcb.8b12561

[24] P. G. Seybold and M. Gouterman, Porphyrins: XIII: Fluorescence spectra and quantum yields, *J. Mol. Spectrosc*., 1969, **31**, 1–13. doi: 10.1016/0022-2852(69)90335-X

[25] T. N. Singh-Rachford and F. N. Castellano, Photon upconversion based on sensitized triplet–triplet annihilation, *Coord. Chem. Rev*., 2010, **254**, 2560–2573. doi: 10.1016/j.ccr.2010.01.003

[26] Z. Wang, M. Ivanov, Y. Gao, L. Bussotti, P. Foggi, H. Zhang, N. Russo, B. Dick, J. Zhao, M. Di Donato, G. Mazzone, L. Luo and M. Fedin, Spin–Orbit Charge-Transfer Intersystem Crossing (ISC) in Compact Electron Donor–Acceptor Dyads: ISC Mechanism and Application as Novel and Potent Photodynamic Therapy Reagents, *Chem. – Eur. J*., 2020, **26**, 1091–1102. doi: 10.1002/chem.201904306

[27] T. W. Ebbesen, K. Tanigaki and S. Kuroshima, Excited-state properties of C_{60}, *Chem. Phys. Lett.,* 1991, **181**, 501–504. doi: 10.1016/0009-2614(91)80302-E

[28] M. Montalti, A. Credi, L. Prodi and M. T. Gandolfi, Handbook of Photochemistry, CRC Press, 2006.

[29] A. Sagadevan, K. C. Hwang and M. -D. Su, Singlet oxygen-mediated selective C–H bond hydroperoxidation of ethereal hydrocarbons, *Nat. Commun.,* 2017, **8**, 1–8. doi: 10.1038/s41467-017-01906-5

[30] M. Gouterman, Spectra of Porphyrins*, *J. Mol. Spectrosc.,* 1961, **6**, 138–163. doi: 10.1016/0022-2852(61)90236-3

[31] M. Kasha, In Spectroscopy of the Excited State.; Di Bartolo, B., Ed.; Plenum Press: New York, 1975, p 340.

[32] B. Dong, C. H. Galka, L. H. Gade, L. Chi and R. M. Williams, Hydrogen-bond Assisted Formation of Rod Shaped Organic Nanocrystals: Control of the Aggregational State and Structural Elucidation, *Nanopages*, 2006, **3**, 325–338. doi: 10.1556/NANO.1.2006.3.4

[33] F. Würthner, T. E. Kaiser and C. R. Saha-Möller, J Aggregates: From Serendipitous Discovery to Supramolecular Engineering of Functional Dye Materials, *Angew. Chem. Int. Ed.,* 2011, **50**, 3376–3410. doi: 10.1002/anie.201002307

[34] N. Keller, M. Calik, D. Sharapa, H. R. Soni, P. M. Zehetmaier, S. Rager, F. Auras, A. C. Jakowetz, A. Görling, T. Clark and T. Bein, Enforcing Extended Porphyrin J-Aggregate Stacking in Covalent Organic Frameworks, *J. Am. Chem. Soc.,* 2018, **140**, 16544–16552. doi: 10.1021/jacs.8b08088.

[35] N. Venkatramaiah, B. Ramakrishna, R. Venkatesan, F. A. Almeida Paz and J. P. C. Tomé, Facile synthesis of highly stable BF3-induced meso-tetrakis (4-sulfonato phenyl) porphyrin (TPPS4)-J-aggregates: structure, photophysical and electrochemical properties, *New J. Chem.*, 2013, **37**, 3745–3754. doi: 10.1039/C3NJ00482A

[36] L. L. Liu, Y. F. Zhao and W. J. Jin, Investigation on the effect of water on the spectroscopic behaviors of TPPS in acidic imidazolium-based ionic liquids, *J. Porphyr. Phthalocyanines*, 2012, **16**, 1132–1139. doi: 10.1142/S1088424612501118
[37] C. -P. Jellen and H. Bettermann, Unusual emissions from low-concentrated porphyrin solutions, *Spectrochim. Acta. A. Mol. Biomol. Spectrosc*., 2003, **59**, 463–470. doi: 10.1016/s1386-1425(02)00214-7
[38] H. Ma, S. Sun, X. Chen, D. Wu, P. Zhu, B. Du and Q. Wei, Spectroscopic studies of aggregation behavior of meso -tetra(4-hydroxyphenyl)porphyrin in aqueous AOT solution, *J. Porphyr. Phthalocyanines*, 2008, **12**, 101–108. doi: 10.1142/S1088424608000133
[39] Q. Han, C. Wang, Z. Li, J. Wu, P. K. Liu, F. Mo and Y. Fu, Multifunctional Zinc Oxide Promotes Electrochemiluminescence of Porphyrin Aggregates for Ultrasensitive Detection of Copper Ion, *Anal. Chem*., 2020, **92**, 3324–3331. doi: 10.1021/acs.analchem.9b05262
[40] I. B. Zakharova, M. A. Elistratova, N. M. Romanov and O. E. Kvyatkovskii, Specific Features of the Electron Structure of ZnTPP Aggregated Forms: Data of Optical Measurements and Quantum-Chemical Calculations, *Semiconductors*, 2018, **52**, 1708–1714. doi: 10.1134/S1063782618130237
[41] N. Hananya, O. Green, R. Blau, R. Satchi-Fainaro and D. Shabat, A Highly Efficient Chemiluminescence Probe for the Detection of Singlet Oxygen in Living Cells, *Angew. Chem. Int. Ed.*, 2017, **56**, 11793–11796. doi: 10.1002/anie.201705803.

[42] F. Wilkinson, W. P. Helman and A. B. Ross, Rate constants for the decay and reactions of the lowest electronically excited singlet state of molecular oxygen in solution. An expanded and revised compilation, *J. Phys. Chem. Ref. Data*, 1995, **24**, 663–677. doi: 10.1063/1.555965
[43] N. Hananya, O. Green, R. Blau, R. Satchi-Fainaro and D. Shabat, A Highly Efficient Chemiluminescence Probe for the Detection of Singlet Oxygen in Living Cells, *Angew. Chem. Int. Ed.*, 2017, **56**, 11793–11796. https://doi.org/10.1002/anie.201705803.

[44] J. N. Demas and G. A. Crosby, The Measurement of Photoluminescence Quantum Yields. A Review, *Am. J. Phys. Chem.,* 1971, **75**, 991–1024. doi: 10.1021/j100678a001
[45] Origin, Version 2018b. OriginLab Corporation, Northampton, MA, USA.
[46] T. Kumpulainen, B. H. Bakker, M. Hilbers and A. M. Brouwer, Synthesis and Spectroscopic Characterization of 1,8-Naphthalimide Derived “Super” Photoacids, *J. Phys. Chem. B*., 2015, **119**, 2515–2524. doi: 10.1021/jp508334s
[47] Igor Pro (Wavemetrics, Lake Oswego, OR, USA).
[48] M. K. Green, C. J. Medforth, C. M. Muzzi, D. J. Nurco, K. M. Shea, K. M. Smith, C. B. Lebrilla and J. A. Shelnutt, Application of matrix-assisted laser desorption/ionization Fourier transform massspectrometry to the analysis of planar porphyrins and highly substituted nonplanar porphyrins, *Eur. Mass Spectrom.,* 1997, **3**, 439–451. doi: 10.1255/ejms.178